ENGINEERING DEVELOPMENT OF SLURRY BUBBLE COLUMN REACTOR (SBCR) TECHNOLOGY

Quarterly Technical Progress Report No. 18

For the Period 1 July – 30 September 1999

Final

Contractor
AIR PRODUCTS AND CHEMICALS, INC.
7201 Hamilton Blvd.
Allentown, PA 18195-1501

Bernard A. Toseland, Ph.D.
Program Manager and Principal Investigator

Daniel J. Driscoll, Ph.D.
Contracting Officer's Representative

Prepared for the United States Department of Energy
Under Cooperative Agreement No. DE-FC22-95PC95051
Contract Period 3 April 1995 – 2 April 2000
Government Award - $797,331 for 3 April 1995 – 2 April 1996

NOTE: AIR PRODUCTS DOES NOT CONSIDER ANYTHING IN THIS REPORT TO BE CONFIDENTIAL OR PATENTABLE.

ENGINEERING DEVELOPMENT OF SLURRY BUBBLE COLUMN REACTOR (SBCR) TECHNOLOGY

Quarterly Technical Progress Report No. 18
For the Period 1 July – 30 September 1999

Contract Objectives

The major technical objectives of this program are threefold: 1) to develop the design tools and a fundamental understanding of the fluid dynamics of a slurry bubble column reactor to maximize reactor productivity, 2) to develop the mathematical reactor design models and gain an understanding of the hydrodynamic fundamentals under industrially relevant process conditions, and 3) to develop an understanding of the hydrodynamics and their interaction with the chemistries occurring in the bubble column reactor. Successful completion of these objectives will permit more efficient usage of the reactor column and tighter design criteria, increase overall reactor efficiency, and ensure a design that leads to stable reactor behavior when scaling up to large diameter reactors.

THE OHIO STATE UNIVERSITY

The report from Ohio State University for the period follows.

INTRINSIC FLOW BEHAVIOR IN A SLURRY BUBBLE COLUMN UNDER HIGH PRESSURE AND HIGH TEMPERATURE CONDITIONS

Quarter Report

(**Reporting Period:** July 1 to September 30, 1999)

Mechanisms of Single Bubble Formation in Liquid-Solid Suspensions at High Pressures with Pressure Fluctuations in the Gas Chamber

Highlights

- The behavior of bubble formation from a single orifice connected to a gas chamber in a non-aqueous liquid and a liquid-solid suspension at high pressures (up to 8.3 MPa) was investigated. The bubble formation from a submerged single orifice connected to a gas chamber was mainly divided into two conditions according to the dimensionless capacitance number: constant flow conditions and variable flow conditions.

- An optic fiber probe was used to measure the bubbling frequency and initial bubble size in liquid-solid suspensions. A high-speed video camera was employed to capture the images of bubbles emerging from the orifice and to measure the frequency of bubble formation in liquids.

- The bubbling frequency was obtained by Fourier analysis of light intensity signals from the optic fiber probe. The bubbling frequency increased with increasing orifice gas velocity and system pressure. The effect of pressure was more significant under variable flow conditions than under constant flow conditions.

- The frequency of bubble formation in the liquid was much higher than in the liquid-solid suspension, especially under high gas velocity conditions. A further increase in solids concentration only slightly reduced the bubbling frequency.

- The effect of pressure on initial bubble size strongly depended on bubble formation conditions. Under variable flow conditions, an increase in pressure significantly reduced the initial bubble size in both the liquid and the liquid-solid suspension. For bubble formation under constant flow conditions, the pressure effect was not significant.

- The bubbles formed in the liquid-solid suspension were larger than those formed in the liquid in the current system under both constant flow and variable flow conditions. A further increase in solids concentration only slightly increased the bubble size.

- A two-stage spherical bubble formation model was extended to describe the bubble formation process in liquid-solid suspensions with pressure fluctuations in the gas chamber. The effects of particle and pressure on bubble motion and pressure balance at the gas-liquid interface were considered in the model.

Work Conducted

Literature Review

Bubble column and slurry bubble column reactors are widely used in industry, particularly in the chemical and petrochemical industries. Many industrial processes of considerable commercial interest, such as methanol synthesis, resid hydrotreating, Fischer-Tropsch synthesis and benzene hydrogenation, are conducted under high pressures. Studies in the literature have indicated significant effects of pressure on hydrodynamics and transport phenomena in bubble columns and slurry bubble columns (Idogowa et al., 1986; Tarmy et al., 1984; Wilkinson, 1991; Inga, 1997; Luo et al., 1999). It is well known that elevated pressures lead to smaller bubble size and narrower bubble size distribution. The bubble size in bubble columns is dictated by three processes: bubble formation, bubble coalescence and bubble breakup. To fully understand the effect of pressure on bubble size, it is necessary to examine the bubble formation process in both liquids and liquid-solid suspensions under high-pressure conditions.

The phenomenon of bubble formation from a submerged single orifice connected to a gas chamber varies with gas injection conditions, which are characterized by the dimensionless capacitance number $N_{c,}$ defined as $4V_c g\rho_l/\pi D_0^2 P_s$ (Kumar and Kuloor, 1970; Tsuge and Hibino, 1983). When N_c is smaller than 1, the gas flow rate through the orifice is constant, which is characterized as constant flow conditions. When N_c is larger than 1, the gas flow rate through the orifice is not constant, and it is dependent on the pressure difference between the gas chamber and bubble. Such bubble formation conditions are characterized as variable flow conditions in this study. Experimental and theoretical studies have examined the effect of pressure or gas density on initial bubble size from a single orifice submerged in liquids under constant flow conditions (Idogawa et al., 1987; Luo et al., 1998a) and under variable flow conditions (LaNauze and Harris, 1974; Tsuge et al., 1992; Wilkinson and van Dierendonck, 1994; Yoo et al., 1998). The high-pressure studies indicate that an increase in gas density or system pressure reduces

the size of bubbles formed from the single orifice. The extent of the pressure effect on initial bubble size depends on bubble formation conditions. Under constant flow conditions, the effect of pressure on initial bubble size is insignificant (Luo et al., 1998a); however, under variable flow conditions, the pressure affects the initial bubble size significantly (Tsuge et al., 1992; Wilkinson and van Dierendonck, 1994).

Although work on bubble formation in liquids at elevated pressures is available in the literature, little is known regarding the fundamental characteristics of bubble formation in liquids containing solid particles. Yoo et al. (1997) investigated the bubble formation process under variable flow conditions in a pressurized system with solid particles. In their experiments, glycerol aqueous solution and 0.1 mm polystyrene beads were used as the liquid and solid phases, respectively. The densities of the liquid and particles were the same; thus, the particles were neutrally buoyant in the liquid and did not induce a particle inertial effect on the bubble. The results of their study indicated that the initial bubble size decreases significantly with increasing pressure. A homogeneous approach quantifying the particle effect was used in their bubble formation model. Both their experimental results and model predictions indicated that particle effect on the initial bubble size was insignificant, which was clearly due to the neutrally buoyant nature of particles used in the study. Luo et al. (1998a) investigated the mechanism of single bubble formation in a slurry system with a significant liquid and particle density difference at pressures up to 17.3 MPa under constant flow conditions. They found that bubbles formed from a single orifice in the liquid-solid suspension were larger than those formed in the liquid, and the initial bubble size increased with increasing solids concentration. The bubble formation model of Luo et al. (1998a) indicated that the particle effect on bubble formation was mainly due to the inertia of the liquid-solid suspension and the collision between the bubbles and particles. It was also found that the pressure effect was insignificant in liquid-solid suspensions under constant flow conditions, similar to the findings that Wilkinson and van Dierendonck (1994) obtained in liquids. The reason is that the effects of pressure on the overall upward forces and overall downward forces governing bubble formation are comparable, and the overall pressure effect is negligible under constant flow conditions. Further work is needed to quantify the effect of pressure on the initial bubble size under variable flow conditions in liquid-solid suspensions.

In this study, the effects of pressure and solids concentration on bubble formation from a single orifice with pressure fluctuations in the gas chamber were examined. Hydrocarbon liquid in the presence and absence of particles was used for the experiments. A mechanistic model was developed to account for the initial bubble size in the liquid-solid suspension under various bubble formation conditions. The mechanisms underlining the particle and pressure effects on bubble formation behavior are discussed in light of the model.

Experimental Setup

The high-pressure, three-phase fluidized bed used in this work for measuring the initial bubble size in liquid-solid suspensions is shown in Figure 1. The fluidized bed is a

stainless steel column, 1.38 m in height and a 0.102-m ID, consisting of three sections, i.e., the plenum, test and disengagement sections. The column can be operated at pressures up to 21 MPa and temperatures up to 180ºC. Three pairs of quartz windows are installed on the front and rear sides of the column. Each window is 12.7 mm wide and 93 mm long.

Nitrogen is injected into the liquid-solid medium through a single orifice 1.63 mm in diameter and 3 mm in thickness. The orifice is attached to a stainless steel gas chamber with a volume of 650 cm^3 through a 3/8-inch tube; tube length is 0.12 m. The flow rate of nitrogen is controlled by adjusting a metering valve and is measured by a mass flow meter. The liquid phase is in batch operation. The particles are suspended by the auxiliary gas, which enters the column through a ring distributor surrounding the tube. After the particles are fully suspended, the auxiliary gas is shut off, and the measurement is conducted before the particles start to settle. The height of the suspension is maintained at 0.4 m from the distributor.

In this study, the liquid phase is Paratherm NF heat transfer fluid. The physical properties of the gas and liquid phases vary with pressure. The particles are glass beads of 210 μm in diameter and 2450 kg/m^3 in density. The system pressure and solids concentration vary in the ranges of 0.1~8.3 MPa and 0~30 vol %, respectively. The orifice gas velocity varies up to the jetting regime.

An optic fiber probe is used to detect bubbles. The probe utilizes the difference in refractive indexes between the gas and liquid phases to distinguish the gas phase from liquid-solid suspensions. Through Fourier analysis of the light intensity signals obtained from the probe, the frequency of bubble formation can be obtained. The details of the probe are given elsewhere (Luo et al., 1998b). In order to verify the validity of this measuring technique, a high-speed video camera (240 frames/s) is used to capture the images of bubbles emerging from the orifice in liquids, and the bubbling frequency is obtained by counting the number of bubbles during a fixed time interval. The bubble frequencies measured by these two techniques are almost identical. By assuming that bubbles are the same size, the volume of a single bubble can be calculated by dividing the gas flow rate into the chamber by the measured bubbling frequency.

Bubbling Frequency

Typical signals of light intensity from the optic fiber probe in a pressurized slurry system are shown in Figure 2(a). The discrete peaks in the time domain indicate the passage of bubbles over the probe. The power spectra of signals obtained by the Fourier analysis are shown in Figure 2(b). As can be seen from the figure, the dominant frequency in the frequency domain corresponds to the frequency of bubble formation. Figures 3 and 4 show the frequency of bubble formation in the liquid and in the liquid-solid suspension under various pressure and solids concentration conditions. As shown in the figures, the bubbling frequency increases with increasing orifice gas velocity. The effect of pressure on the bubbling frequency can be seen in Figure 3. For bubble formation in both the liquid and the liquid-solid suspension, elevated pressures lead to higher bubbling

frequency. The pressure effect is more significant in the pressure range of 0.1 to 2.5 MPa, in which the bubble formation is under variable flow conditions (N_c>1). When the pressure is further increased, the bubble formation may be under constant flow conditions (N_c≤1), and the change of bubbling frequency with pressure is not significant.

The effect of solids concentration on bubbling frequency is shown in Figure 4. The frequency of bubble formation in the liquid is much higher than that in the liquid-solid suspension, especially under high gas velocity conditions. This implies that the initial bubble size in the slurry is much larger than that in the liquid at the same conditions for the present system. However, for bubbles formed in the liquid-solid suspension, a further increase in solids concentration only slightly reduces the bubbling frequency under high gas velocity conditions. It is also found that the variation of bubbling frequency with orifice gas velocity depends on bubble formation conditions. For bubble formation under variable flow conditions as shown in Figure 4(a), the variation of bubbling frequency with orifice gas velocity is almost linear. For bubble formation under constant flow conditions as shown in Figure 4(b), at low gas velocities, the bubbling frequency increases linearly with gas velocity and appears not to be influenced by the solids concentration. Above a certain gas velocity, the rate of increase of bubbling frequency with gas velocity becomes smaller and the frequency decreases with increasing solids concentration.

Initial Bubble Size

Pressure Effect

A sequence of bubble images showing the process of bubble formation in liquids at the elevated pressure is shown in Figure 5. It can be seen that a bubble growing at the orifice remains roughly spherical until it detaches from the orifice. The two stages in the bubble formation process, i.e., the expansion stage and the detachment stage, can be seen clearly in Figure 5. Thus, the two-stage spherical model is justifiable for use in the simulation of bubble formation process. The experimental data of the initial bubble size in the liquid and liquid-solid suspension under various pressures are shown in Figure 6. It is found that the pressure effect on the initial bubble size is strongly affected by the bubble formation conditions. Under variable flow conditions (N_c>1), an increase in pressure significantly reduces the initial bubble size in both the liquid and the liquid-solid suspension. For bubble formation under constant flow conditions (N_c≤1), the pressure effect is not significant, which is consistent with the findings of Wilkinson and van Dierendonck (1994), Yoo et al. (1997) and Luo et al. (1998a) for bubble formation in the liquid. For example, at the orifice gas velocity of 1.0 m/s and a solids concentration of 18 vol %, the initial bubble size decreases from 1.09 to 0.76 cm (30% decrease) when the pressure increases from 0.1 to 0.7 MPa; however, at the same gas velocity and solids concentration, the initial bubble size only changes from 0.53 to 0.51 cm (4% decrease) when the pressure increases from 2.5 to 8.3 MPa.

Particle Effect

Figure 7 shows the particle effect on the initial bubble size under various bubble formation conditions. For bubble formation under both constant flow and variable flow

conditions, the bubbles formed in the liquid-solid suspension are larger in size than those formed in the liquid at a given gas velocity for the present system. For bubble formation in the liquid-solid suspension, a further increase in solids concentration only slightly increases bubble size. The particles yield resistant forces for the detachment of bubbles, resulting in longer bubble formation time and hence larger bubble size.

Mathematical Model

A two-stage, spherical bubble formation model (Ramakrishnan et al., 1969; Tsuge and Hibino, 1978; Luo et al., 1998a) is extended in this study to describe the bubble formation process in liquid-solid suspensions with pressure fluctuations in the gas chamber. In the two-stage model, bubbles are assumed to be formed in two stages, namely, the expansion stage and the detachment stage. The bubble expands with its base attached to the orifice during the expansion stage. In the detachment stage, the bubble base moves away from the orifice and remains connected to the orifice through a neck. The shape of the bubble is assumed to remain spherical in the entire bubble formation process. It is also assumed in this model that a liquid film always exists around the bubble. During the expansion and detachment stages, particles collide with the bubble and stay on the liquid film. The particles and the liquid surrounding the bubble are displaced and set in motion by the bubble as the bubble grows and rises. The schematic diagram of bubble formation is shown in Figure 8.

Luo et al. (1998a) successfully extended the two-stage spherical bubble formation model to simulate bubble formation in liquid-solid suspensions under constant flow conditions. In order to extend this model to simulate bubble formation in liquid-solid suspensions under variable flow conditions, particle effects on bubble motion and pressure balance at the bubble-liquid interface need to be considered. A detailed description of model equations and modifications of the model are provided below.

Bubble Motion Equation

The motion equation of a rising bubble in liquid-solid suspensions can be described based on a balance of all the forces acting on the bubble (Luo et al., 1998a). The forces induced by the liquid include the upward forces [effective buoyancy (F_B) and gas momentum (F_M) forces], and the downward resistance [liquid drag (F_D), surface tension force (F_σ), bubble inertial force ($F_{I,g}$), and Basset force (F_{Basset})]. Two other downward forces on the bubble account for the particle effect on the bubble motion, i.e., the particle-bubble collision force (F_C) and the suspension inertial force ($F_{I,m}$), due to the acceleration of the liquid and particles surrounding the bubble (Luo et al., 1998a). Therefore, the overall force balance on the bubble formed in liquid-solid suspensions can be written as

$$F_B + F_M = F_D + F_\sigma + F_{Basset} + F_{I,g} + F_C + F_{I,m}\,. \qquad (1)$$

The expansion and detachment stages follow the same force balance equation (Eq. (1)), although the expressions for the same force in two stages may be different. The expressions for all the forces under two stages are given in Table 1. The particle-bubble

collision force is merely the rate of momentum change of particles colliding with the bubble surface. The suspension inertial force can be derived from the suspension flow field around an accelerating bubble. Luo et al. (1998a) quantified the flow field of the suspension around a two-dimensional bubble by using the Particle Image Velocimetry (PIV) technique and obtained the expression for the suspension inertial force, $F_{I,,m}$:

$$F_{I,m} = \frac{d\left(\iiint \rho_m u_m \delta V\right)}{dt} = \zeta \frac{d}{dt}\left[\rho_m \left(\frac{4}{3}\pi r_b^3\right) u_b\right] \qquad (2)$$

where the apparent density of the suspension is defined as:

$$\rho_m = \varepsilon_s \rho_s + \varepsilon_l \rho_l . \qquad (3)$$

For bubbles formed in liquid-solid suspensions, the coefficient ζ is equal to 3.86 (Luo et al., 1998a). When bubbles are formed in liquids, the coefficient ζ is equal to $\frac{11}{16}$, corresponding to the added mass in inviscid liquids (Milne-Thomson, 1955). The detailed descriptions of these forces are given in Luo et al. (1998a).

In the expansion stage, the rise velocity of the bubble, u_b, is equal to the bubble expansion velocity, i.e.,

$$u_b = u_e = \frac{dr_b}{dt} \qquad (4)$$

and the gas flow rate through the orifice, Q_0, can be expressed by the following equation:

$$Q_0 = \frac{dV_b}{dt} = 4\pi r_b^2 \frac{dr_b}{dt} . \qquad (5)$$

Substituting the expressions of various forces in Table 1 into Eq. (1) and considering Eqs. (4)~(5), the force balance at the end of the expansion stage can be written as:

$$\frac{d}{dt}\left[\left(\rho_g + \zeta\rho_m\right)\left(\frac{4}{3}\pi r_b^3\right)\frac{dr_b}{dt}\right] = \frac{4\pi r_b^3}{3}\left(\rho_l - \rho_g\right)g + \frac{\rho_g Q_0^2}{\frac{1}{4}\pi D_0^2} - 6\pi\mu_l r_b \frac{dr_b}{dt} - \pi D_0 \sigma \cos\gamma - \frac{1}{4}\pi D_0^2 \rho_s \varepsilon_s \left(\frac{dr_b}{dt}\right)^2 \qquad (6)$$

The term on the left-hand side represents the inertial forces of the bubble and suspension. The five terms on the right-hand side represent the buoyancy, gas momentum, viscous, surface tension and particle-bubble collision forces, respectively.

In the detachment stage, the rise velocity of the bubble is the sum of the expansion velocity (u_e) and the bubble base rising velocity (u):

$$u_b = u + u_e = \frac{dx}{dt} \tag{7}$$

where x is the vertical distance between the bubble center and orifice plate. The gas flow rate through the orifice can be expressed by:

$$Q_0 = \frac{d(V_b + V_{neck})}{dt} = \frac{d\left[\frac{4}{3}\pi r_b^3 + \frac{1}{4}\pi D_0^2 (x - r_b)\right]}{dt} = 4\pi r_b^2 \frac{dr_b}{dt} + \frac{1}{4}\pi D_0^2 \left(\frac{dx}{dt} - \frac{dr_b}{dt}\right). \tag{8}$$

Then, the motion equation of a bubble in the detachment stage can be written as follows:

$$\frac{d}{dt}\left[\left(\rho_g + \zeta\rho_m\right)\left(\frac{4}{3}\pi r_b^3\right)\frac{dx}{dt}\right] = \frac{4\pi r_b^3}{3}\left(\rho_l - \rho_g\right)g + \frac{\rho_g Q_0^2}{\frac{1}{4}\pi D_0^2} - 6\pi\mu_l r_b \frac{dx}{dt} - \pi D_0 \sigma \cos\gamma$$
$$- \pi r_b^2 \rho_s \varepsilon_s \left(\frac{d(x - r_b)}{dt}\right)^2 - 12 r_b^2 \sqrt{\pi\rho_l \mu_l t}\, \frac{d^2(x - r_b)}{dt^2} \tag{9}$$

The terms on the right-hand side represent the buoyancy, gas momentum, viscous, surface tension, particle-bubble collision and Basset forces, respectively. The other model equations will be presented later.

Notations

C_D	drag coefficient, dimensionless
D_0	orifice diameter, m
d_b	initial bubble size, m
e	restitution coefficient, dimensionless
F_σ	surface tension force, N
f_b	bubbling frequency, Hz
F_B	buoyancy force, N
F_{Basset}	Basset force, N
F_C	particle-bubble collision force, N
F_D	liquid drag force, N
$F_{I,g}$	bubble inertial force, N
$F_{I,m}$	suspension inertial force, N
F_M	gas momentum force, N
g	gravitational acceleration, m/s^2
h	liquid level in the column, m
N_c	capacitance number, dimensionless
P_b	pressure in the bubble, Pa
P_c	pressure in the gas chamber, Pa

P_e pressure at the gas inlet to the chamber, Pa
P_s system pressure, Pa
Q_0 instantaneous gas flow rate through the orifice, m^3/s
Q_g volumetric gas flow rate entering the gas chamber, m^3/s
r_b bubble radius, m
Re Reynolds number, $\frac{2\rho_l u_b r_b}{\mu_l}$, dimensionless
T temperature, K
t time, s
u rise velocity of bubble base, m/s
u_0 instantaneous gas velocity through the orifice, m/s
u_b rise velocity of bubble center, m/s
u_e bubble expansion velocity, m/s
u_g orifice gas velocity, m/s
u_m velocity of liquid-solid suspensions, m/s
V_b volume of bubble, m^3
V_c volume of gas chamber, m^3
V_{neck} volume of neck, m^3
x distance between bubble center and orifice plate, m
ρ_g gas density, kg/m^3
ρ_l liquid density, kg/m^3
ρ_m density of liquid-solid suspensions, kg/m^3
ρ_s particle density, kg/m^3
ε_l liquid holdup, dimensionless
ε_s solids concentration, dimensionless
μ_l liquid viscosity, Pa·s
γ contact angle between bubble surface and orifice, rad
σ surface tension, N/m
ζ coefficient in Eq. (2), dimensionless

References

Idogawa, K., K. Ikeda, and T. Fukuda, "Formation and flow of gas bubbles in a pressurized bubble column with a single orifice or nozzle gas distributor," *Chem. Eng. Comm.*, **59**, 201 (1987).

Idogawa, K., K. Ikeda, T. Fukuda, and S. Morooka, "Behavior of bubbles of the air-water system in a column under high pressure," *Int. Chem. Eng.*, **26**, 468 (1986).

Inga, J. R., *Scaleup and Scaledown of Slurry Reactors: A New Methodology*, Ph.D. thesis, University of Pittsburgh, Pa. (1997).

Kumar, R., and N. R. Kuloor, "The formation of bubbles and drops," *Advances in Chemical Engineering*, **8**, 255 (1970).

LaNauze, R. D., and I. J. Harris, "Gas bubble formation at elevated system pressures," *Trans. Instn. Chem. Engrs.*, **52**, 337 (1974).

Luo, X., D. J. Lee, R. Lau, G. Q. Yang, and L. S. Fan, "Maximum stable bubble size and gas holdup in high-pressure slurry bubble columns," *AIChE J.*, **45**, 665 (1999).

Luo, X., G. Q. Yang, D. J. Lee, and L. S. Fan, "Single bubble formation in high pressure liquid-solid suspensions," *Powder Technology*, **100**, 103 (1998a).
Luo, X., K. Tsuchiya, and L. S. Fan, "Gas jetting and bubble formation in high pressure liquid-solid suspensions," in *Fluidization IX*, edited by L. S. Fan and T. M. Knowlton, Engineering Foundation, N.Y., 637 (1998b).
Milne-Thomson, L. M., *Theoretical Hydrodynamics*, 3rd ed., Macmillan and Co. Ltd., London (1955).
Ramakrishnan, S., R. Kumar, and N. R. Kuloor, "Studies in bubble formation – I: Bubble formation under constant flow conditions," *Chem. Eng. Sci.*, **24**, 731 (1969).
Tarmy, B., M. Chang, C. Coulaloglou, and P. Ponzi, "Hydrodynamic characteristics of three phase reactors," *The Chemical Engineer*, October, 18 (1984).
Tsuge, H., and S. Hibino, "Bubble formation from a submerged single orifice accompanied by pressure fluctuations in gas chamber," *J. Chem. Eng. Japan*, **11**, 173 (1978).
Tsuge, H., and S. Hibino, "Bubble formation from an orifice submerged in liquids," *Chem. Eng. Comm.*, **22**, 63 (1983).
Tsuge, H., Y. Nakajima, and K. Terasaka, "Behavior of bubbles formed from a submerged orifice under high system pressure," *Chem. Eng. Sci.*, **47**, 3273 (1992).
Wilkinson, P. M., and L. L. van Dierendonck, "A theoretical model for the influence of gas properties and pressure on single-bubble formation at an orifice," *Chem. Eng. Sci.*, **49**, 1429 (1994).
Wilkinson, P. M., *Physical Aspects and Scale-Up of High Pressure Bubble Columns*, Ph.D. thesis, University of Groningen, The Netherlands (1991).
Yoo, D. H., H. Tsuge, K. Terasaka, and K. Mizutani, "Behavior of bubble formation in suspended solution for an elevated pressure system," *Chem. Eng. Sci.*, **52**, 3701 (1997).
Yoo, D. H., K. Terasaka, and H. Tsuge, "Behavior of bubble formation at elevated pressure," *J. Chem. Eng. Japan*, **31**, 76 (1998).

Table 1 Expressions of the Forces Involved in the Bubble Formation Process (Luo et al., 1998a)

FORCES	EXPANSION STAGE	DETACHMENT STAGE
F_B	$\frac{4\pi}{3} r_b^3 (\rho_l - \rho_g) g$	Same as expansion stage
F_M	$\frac{\pi}{4} D_0^2 \rho_g u_0^2$	Same as expansion stage
F_D	$C_D (\pi r_b^{\,2}) \frac{\rho_l u_b^2}{2} \qquad (C_D = 24/\mathrm{Re})$	Same as expansion stage
F_σ	$\pi D_0 \sigma \cos\gamma$	Same as expansion stage
$F_{I,g}$	$\frac{d}{dt}\left[\rho_g \left(\frac{4}{3}\pi r_b^3\right) u_b\right]$	Same as expansion stage
F_{Basset}	Not applicable	$12 r_b^2 \sqrt{\pi \rho_l \mu_l t}\, \frac{du}{dt}$
F_C	$\frac{\pi}{4} D_0^{\,2} (1+e) \varepsilon_s \rho_s u_e^{\,2}$	$\pi r_b^{\,2} \varepsilon_s \rho_s u^2$
$F_{I,m}$	$\frac{\mathrm{d}(\iiint \rho_\mathrm{m} u_m \delta V)}{\mathrm{d}t} = 3.86 \frac{\mathrm{d}}{\mathrm{d}t}\left[\rho_m \left(\frac{4}{3}\pi r_b^3\right) u_b\right]$	Same as expansion stage

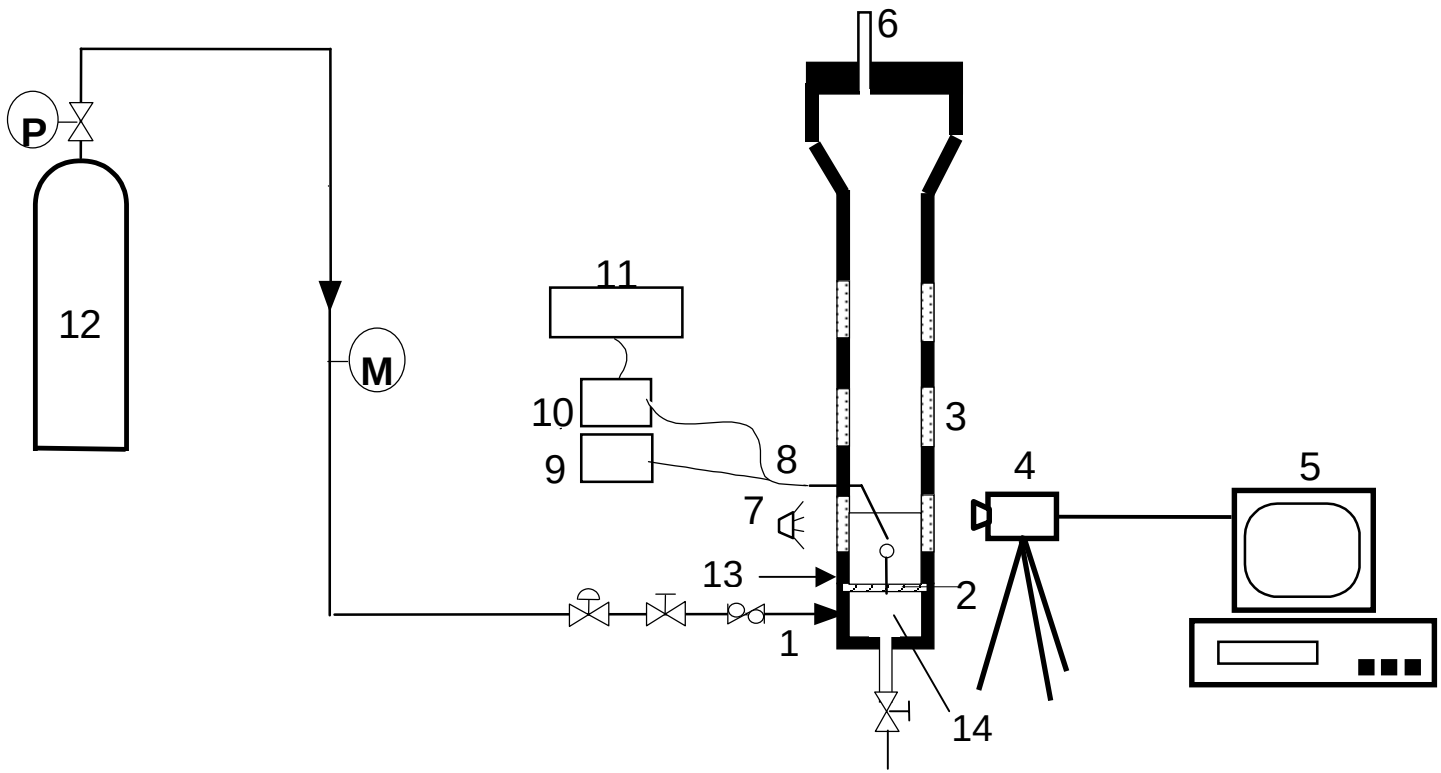

Figure 1 Experimental Setup for the Measurement of Initial Bubble Size in High-Pressure Liquid-Solid Suspensions (1.Gas inlet; 2.Distributor; 3.Quartz windows; 4.High-speed video camera; 5.Monitor and high-speed VCR; 6.Gas outlet; 7.Lighting; 8.Optical fiber probe; 9.Light source; 10.Photomultiplier; 11.Data acquisition system; 12.Nitrogen cylinder; 13.Auxiliary gas inlet; 14.Gas chamber)

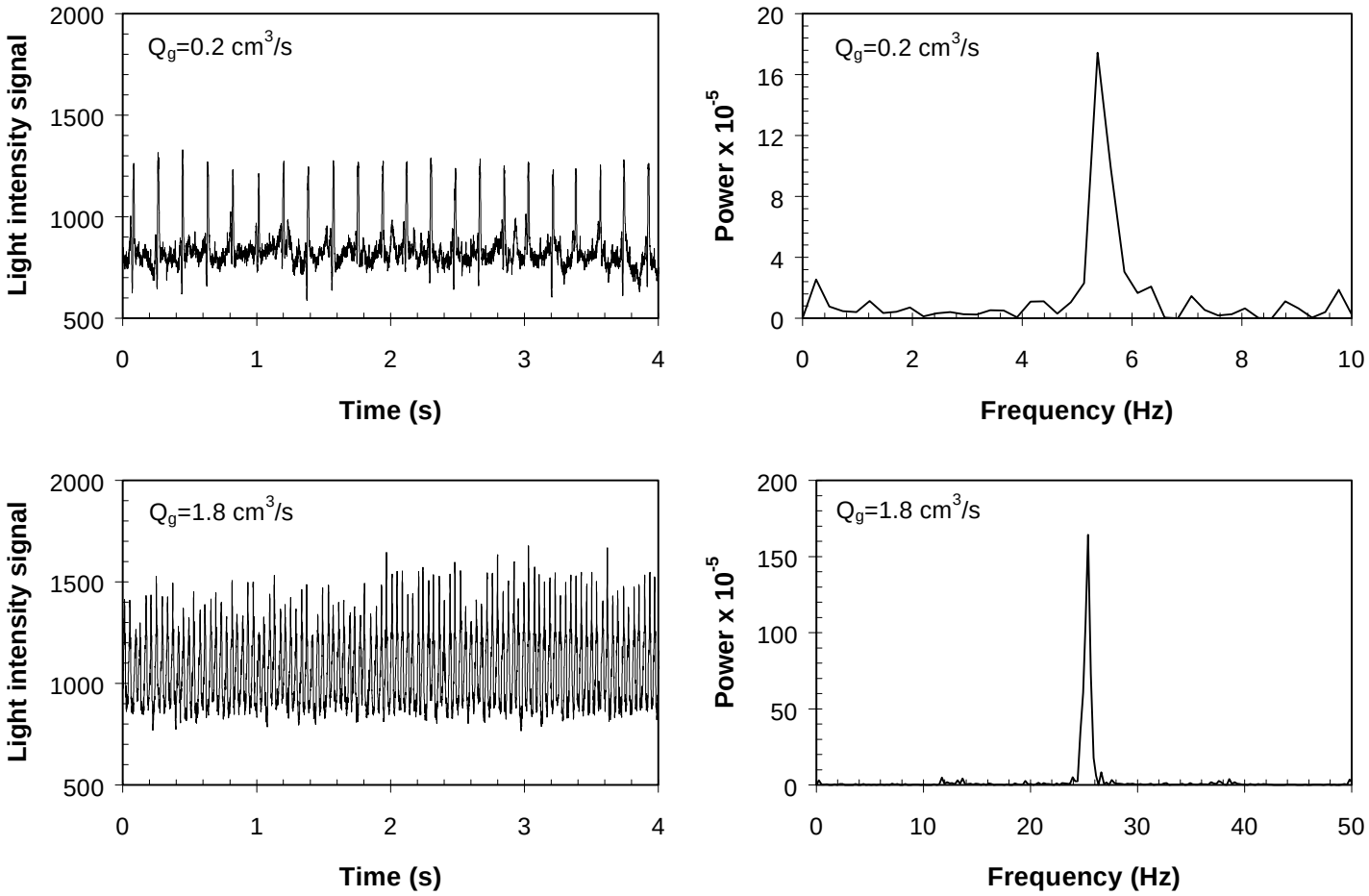

(a) (b)

Figure 2. (a) Typical Signals from the Optic Fiber Probe and (b) Corresponding Power Spectra in a Pressurized Slurry System at Different Gas Flow Rates (P_s=2.5 MPa, ε_s=0.18)

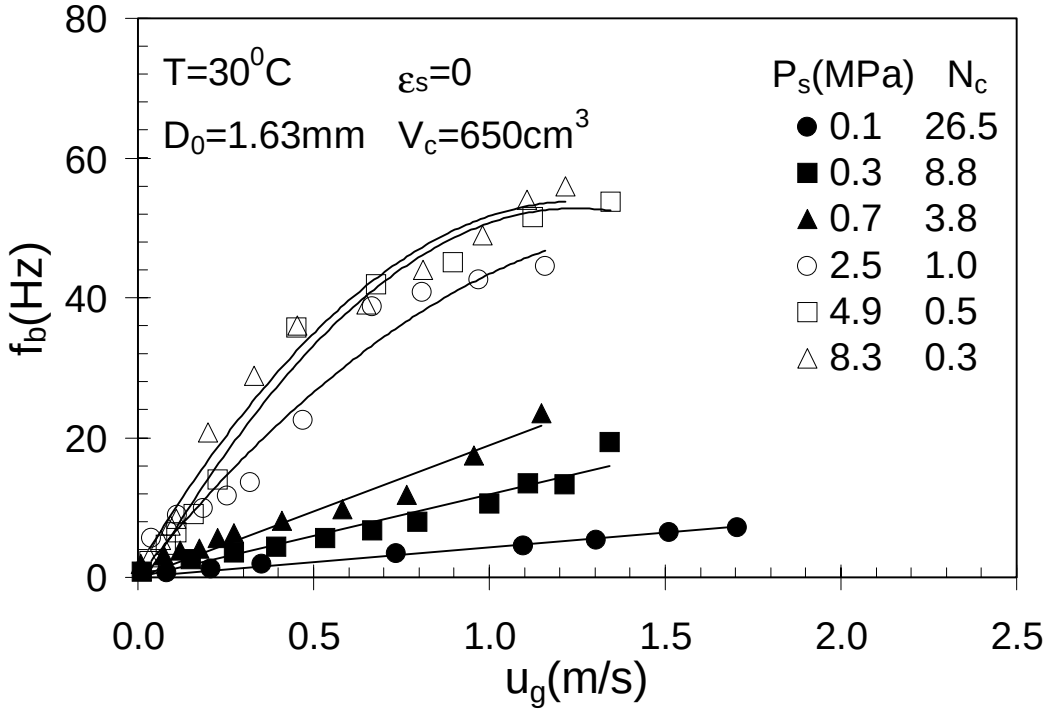

(a)

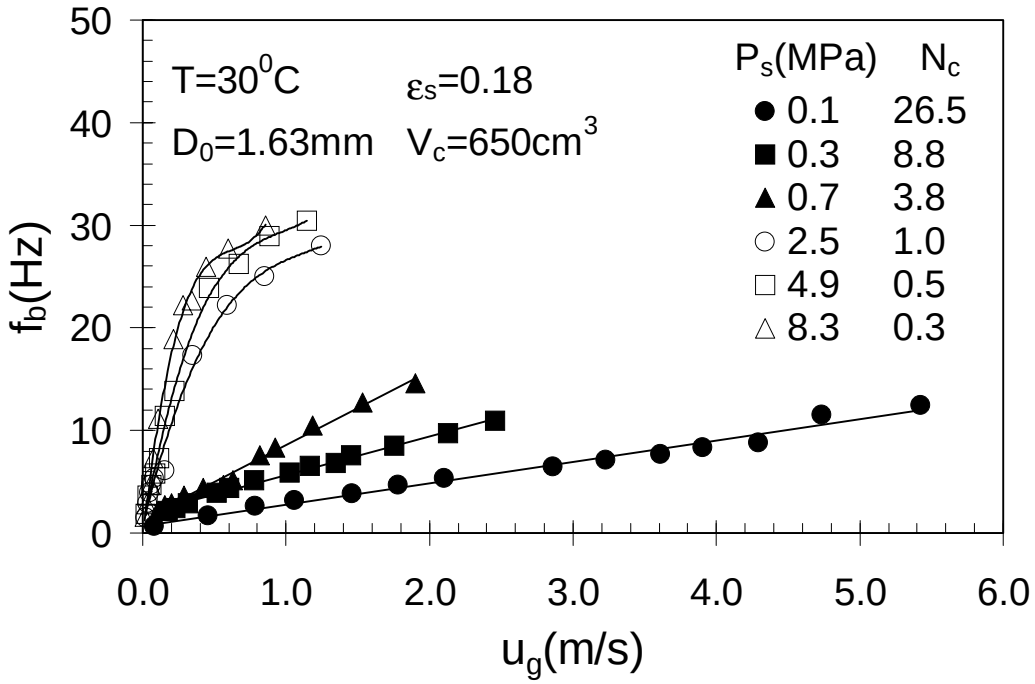

(b)

Figure 3 Effect of Pressure on the Frequency of Bubble Formation from a Single Orifice Accompanied by Pressure Fluctuations in the Gas Chamber ($T=30^0C$, $D_0=1.63mm$, $V_c=650cm^3$): (a) in the liquid ($\varepsilon_s=0$); and (b) in the liquid-solid suspension ($\varepsilon_s=0.18$).

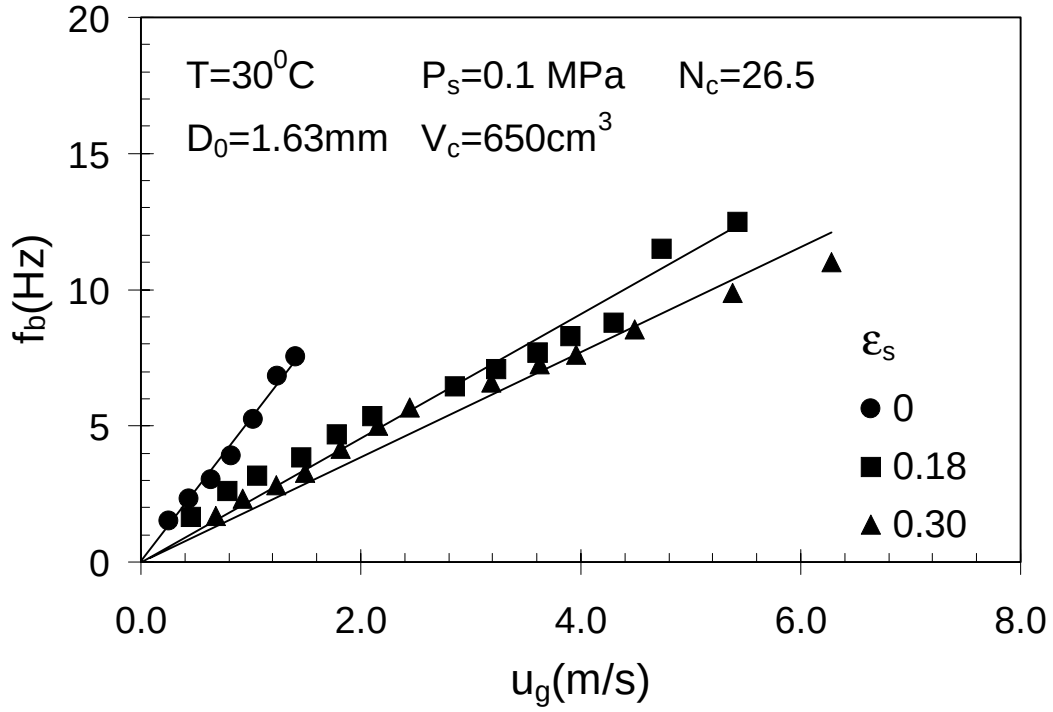

(a)

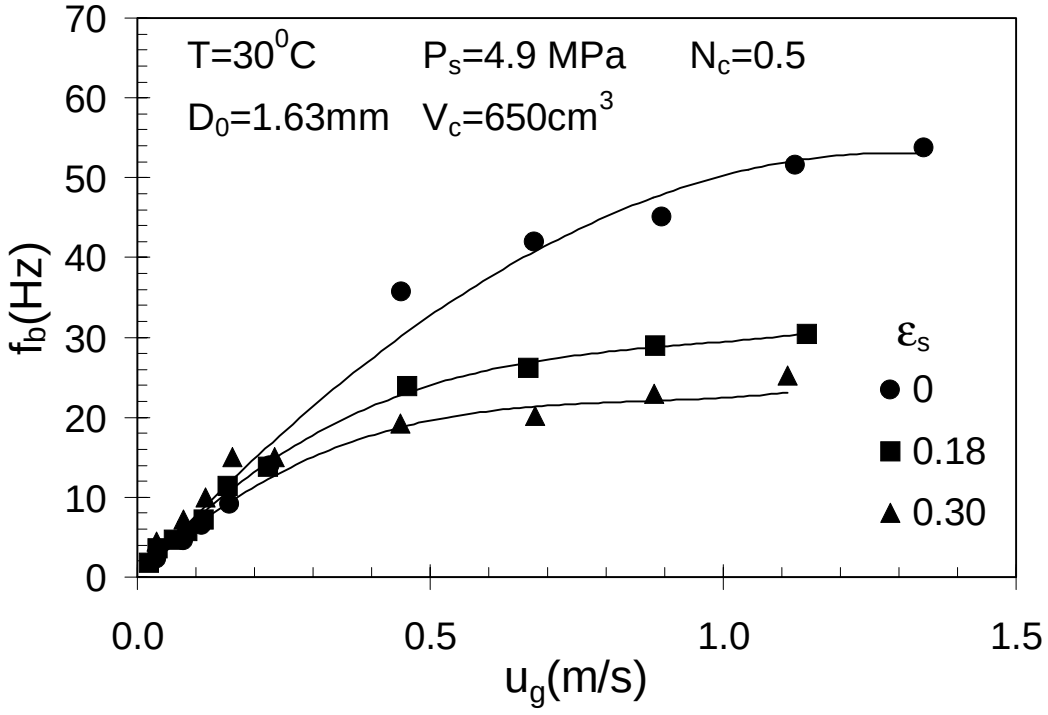

(b)

Figure 4 Effect of Solids Concentration on the Frequency of Bubble Formation from a Single Orifice Accompanied with Pressure Fluctuations in the Gas Chamber (T=30^{0}C, D_0=1.63mm, V_c=650cm^3): (a) variable flow conditions (P_s=0.1MPa, N_c=26.5); and (b) constant flow conditions (P_s=4.9MPa, N_c=0.5).

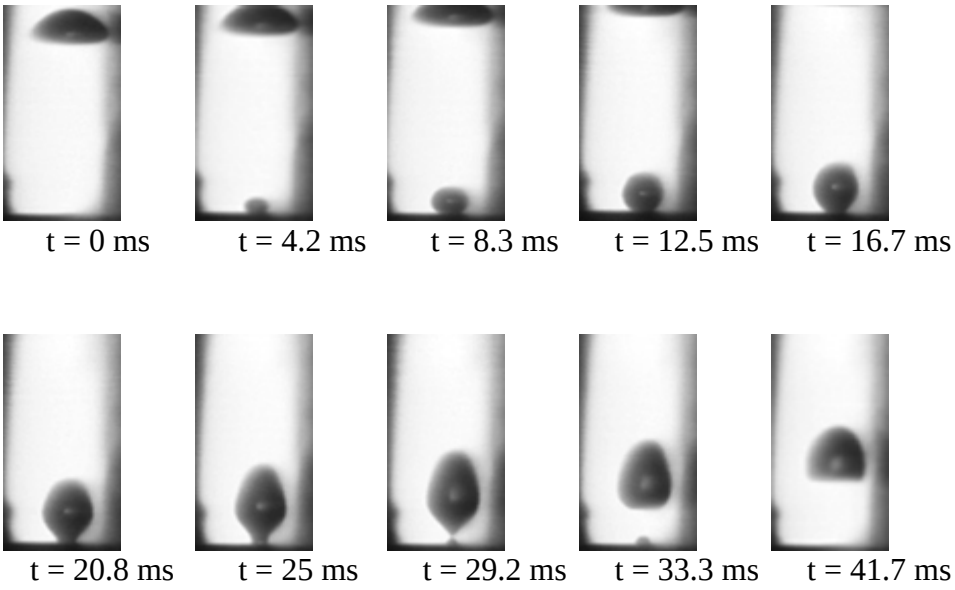

Figure 5 A Sequence of Bubble Images Showing the Process of Bubble Formation in Liquids under High Pressures (P_s=0.7 MPa, Q_g=1.6 cm^3/s)

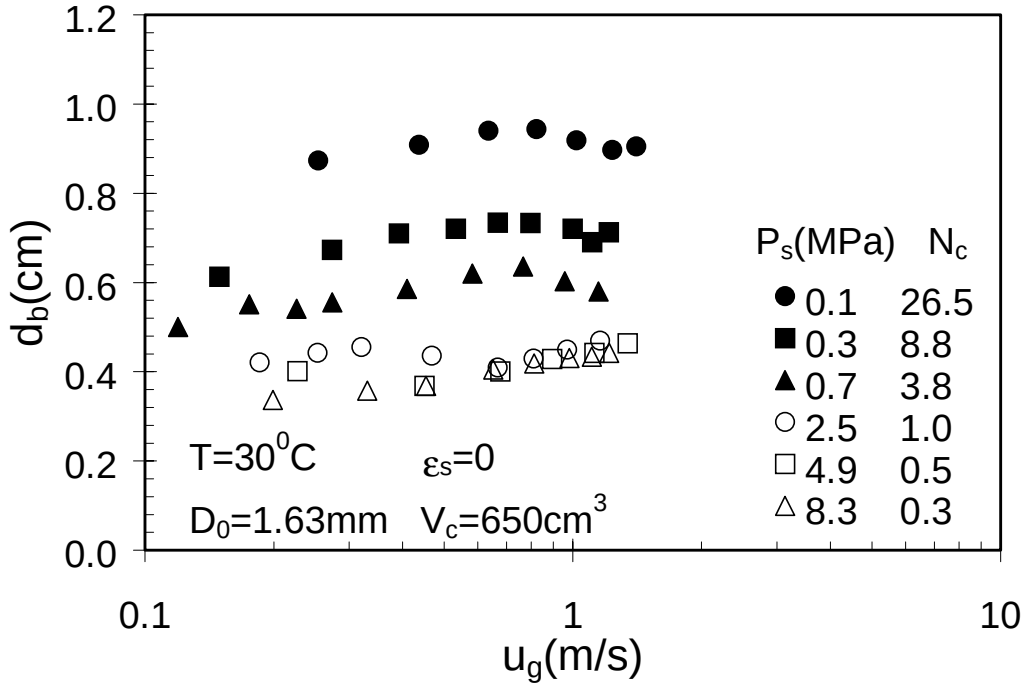

(a)

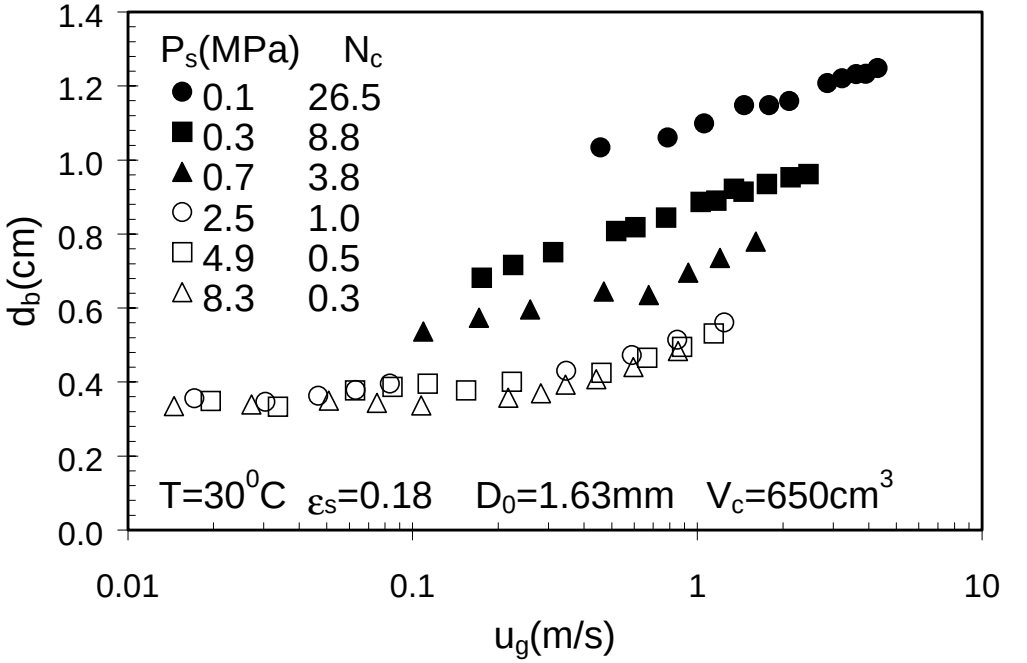

(b)

Figure 6 Effect of Pressure on the Initial Bubble Size (T=30^{0}C, D_0=1.63mm, V_c=650cm^3): (a) in the liquid (ε_s=0); and (b) in the liquid-solid suspension (ε_s=0.18)

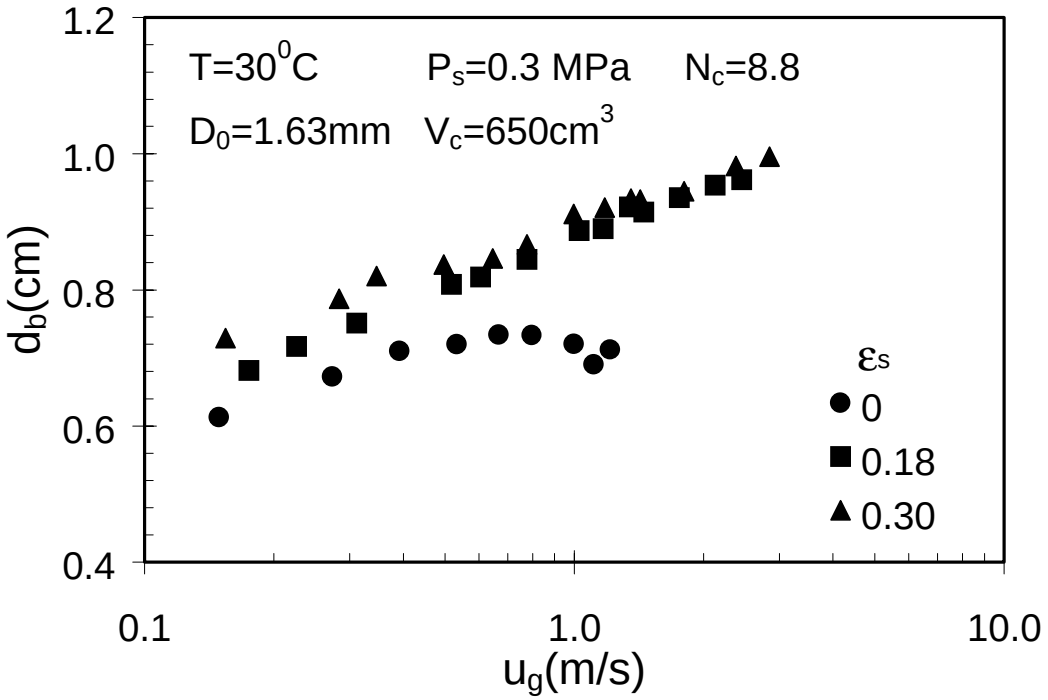

(a)

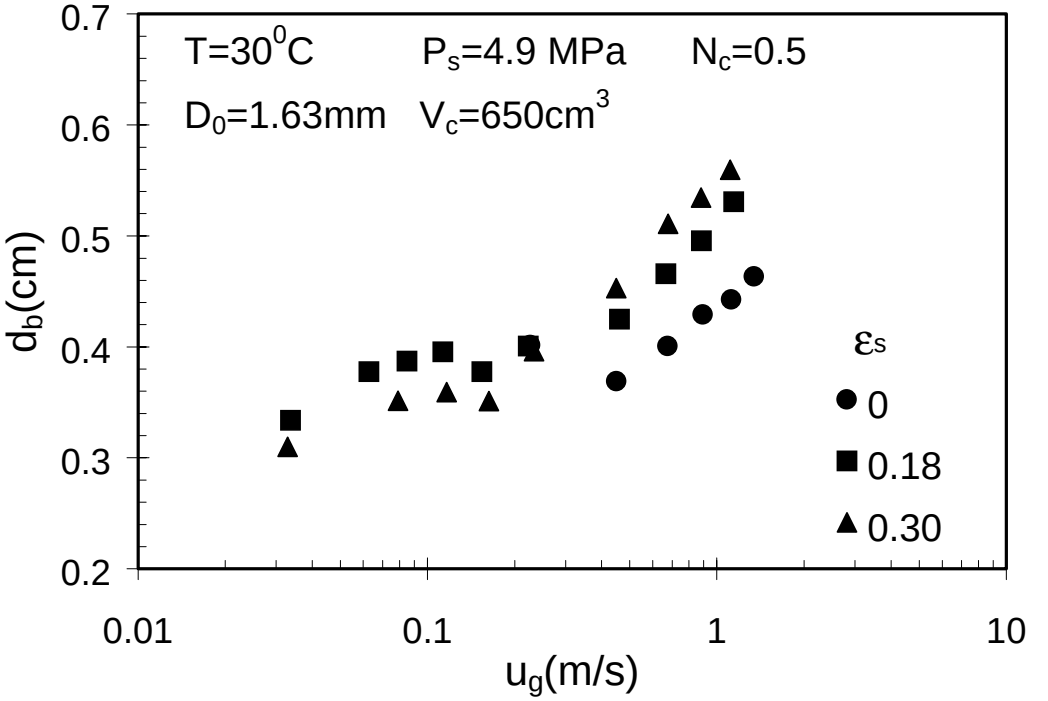

(b)

Figure 7 Effect of Solids Concentration on the Initial Bubble Size (T=30^{0}C, D_0=1.63mm, V_c=650cm^3): (a) variable flow conditions (P_s=0.3MPa, N_c=8.8); and (b) constant flow conditions (P_s=4.9MPa, N_c=0.5)

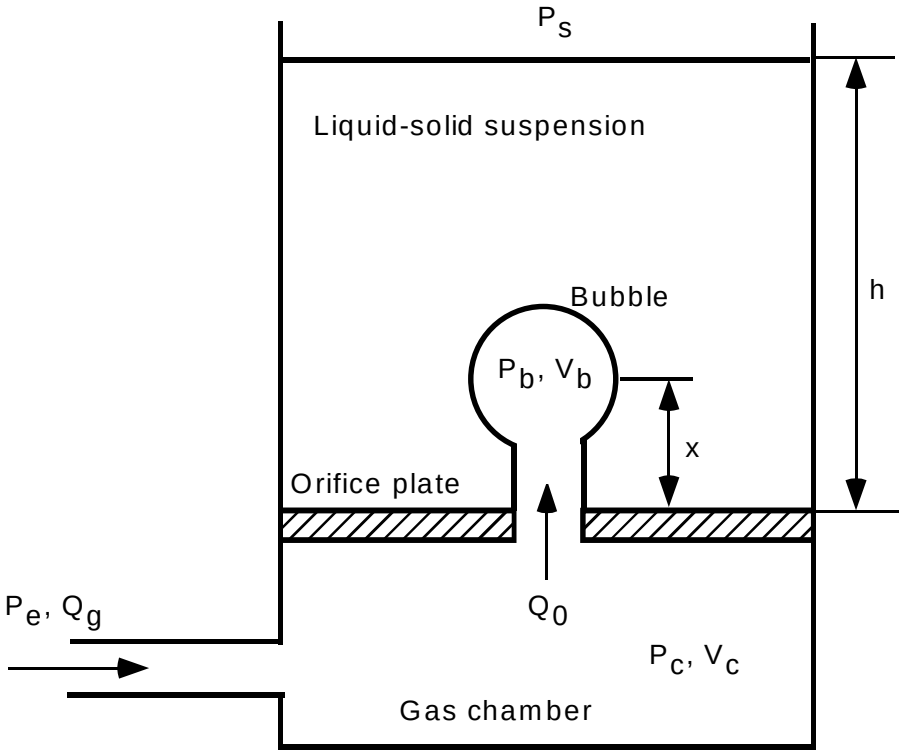

Figure 8 Schematic Diagram of Bubble Formation from a Single Orifice Connected to a Gas Chamber

WASHINGTON UNIVERSITY IN ST. LOUIS

The report from Washington University for the period follows.

ENGINEERING DEVELOPMENT OF SLURRY BUBBLE COLUMN REACTOR (SBCR) TECHNOLOGY

Eighteenth Quarterly Report
for
July 1 - September 30, 1999

(Budget Year 4: October 1, 1998 – September 30, 1999)

Chemical Reaction Engineering Laboratory (CREL)
Chemical Engineering Department
Washington University

Objectives for the Fourth Budget Year

The main goal of this subcontract from the Department of Energy via Air Products is to study the fluid dynamics of slurry bubble columns and address issues related to scaleup and design. The objectives set for the fourth budget year (October 1, 1998 – September 30, 1999) are listed below.

- Extension of CARPT/CT database to conditions of industrial interest such as high superficial gas velocity (up to 30-50 cm/s).
- Examination of the improved gas mixing phenomenological model against LaPorte tracer data.
- Critical evaluation of the developed phenomenological models for liquid and gas mixing against the newly obtained data.
- Testing of the 4-points optical probe for bubble size and bubble rise velocity measurements.
- Further improvement in Computational Fluid Dynamics (CFD) using CFDLIB and FLUENT through development of improved closure schemes and comparison of two-dimensional (2D) and three-dimensional (3D) model predictions with 2D and 3D data.

In this report, the research progress and achievements accomplished in the eighteenth quarter (July 1 - September 30, 1999) are summarized.

Summary of Accomplishments for the Fourth Budget Year

All of the work planned for Year 4 has been accomplished. However, some of the results require significant processing time, and for that reason have not yet been fully reported. This summary cites the results for the Fourth Budget Year that have been discussed in the monthly and quarterly reports and also lists the work completed for which results will be reported soon.

- The Computed Tomography (CT) database for bubble columns (air-water systems) has been extended to superficial gas velocities of up to 60 cm/s at atmospheric conditions. The results will be reported in the near future.

- The effect of sparger design on the gas holdup profile in bubble columns using an air-water system has been studied using CT. Five different distributor designs were used. It was shown that there are no differences in gas holdup profiles generated by various distributors at a high Ug = 30 cm/s. At a lower Ug = 14 cm/s, only industrially relevant spargers (cross sparger, single nozzle) behave the same, while others deviate from each other.

- A one-dimensional (1D), phenomenological, two bubble-class, gas-liquid recirculation model was improved to characterize mixing in both the gas and liquid phase. A 1D sub-model based on the two-fluid approach and the momentum balances for the gas and liquid phase was developed to compute the 1D radial profiles of the time-averaged liquid and gas axial velocities. The model was examined against the radioactive gas tracer runs executed at the LaPorte Alternative Fuels Development Unit (AFDU) during methanol synthesis. The model was used strictly in the predictive sense, with all the parameters estimated independently, and not by fitting tracer data. The model predicts the tracer to be leaving the system faster than the experimentally observed responses. This points out the importance of the precise knowledge of the radial gas holdup profile, since it is this profile that determines the rate of gas and liquid recirculation, and therefore, the average speed of tracer propagation.

- A conductivity measurement technique has been developed to characterize the mixing in bubble columns via the tracer method and to measure gas holdup and bubble rise velocity. Work is in progress to investigate local mixing, gas holdup and bubble rise velocity in the bubble column, and the findings will be reported in the near future. It was found that processing the conductance signals in the bubble column is not straightforward due to the systematic lowering of the conductance of the probe measurement volume when a bubble contacts or is pierced by the probe tip. Therefore, the novel filtering algorithm developed in CREL will be used to cleanly extract the actual liquid phase conductance (which is proportional to the tracer

concentration) from response signals representing the instantaneous point conductance of a bubbling, two-phase, gas-liquid mixture.

- A four-point optical probe for bubble size and bubble rise velocity measurements has been prepared and interfaced with the data acquisition system. Work is in progress to test and implement the four-point optical probe technique in an air-water system.

- Progress was made on the CFD using CFDLIB and Fluent through comparison of 2D and 3D model predictions with existing experimental data in 2D and 3D bubble columns. Reasonably good agreements were obtained between the computed mean quantities, which include liquid velocity, turbulent intensities and Reynolds-like shear stresses, and PIV and CARPT data in 2D and 3D bubble columns.

Objectives for the Fifth Budget Year

The objectives set for the Fifth Budget Year (October 1, 1999 to September 30, 2000) are listed below.

- Extension of the CARPT database to high superficial gas velocity in bubble columns.

- Extension of CARPT/CT database to gas-liquid-solid systems at high superficial gas velocity.

- Evaluation of the effect of sparger design on the fluid dynamics of bubble columns using the CARPT technique.

- Interpretation of LaPorte tracer data.

- Further improvement in Computational Fluid Dynamics (CFD) using CFDLIB and Fluent.

HIGHLIGHTS FOR THE 18TH QUARTER

Distributor Effects in Bubble Columns on Gas Holdup via Computed Tomography (CT)

- Distributor effects on gas holdup have been investigated in a 6.4-in. (16.2-cm) diameter column at atmospheric conditions and at superficial gas velocities of 14 and 30 cm/s.
- The following spargers were studied:
  - Spargers of 0.1% open area (as per the original plan with Sandia National Laboratory)
    - D1: Uniform perforated plate sparger (163 holes, 0.4 mm ID, triangular pitch of 1 cm)
    - D2: Cross sparger (4 holes, 2.6 mm ID)
    - D3: Single nozzle (1 hole, 5.1 mm ID)
  - Additional spargers (developed by a CREL initiative for a comprehensive study of distributors):
    - D4: Uniform perforated plate distributor (163 holes, 0.5 mm ID, triangular pitch of 1 cm, 0.15% open area)
    - D5: Non-uniform perforated plate (61 holes, 0.4 mm ID, 0.04% open area)
- Reproducibility of the measured gas holdup profiles has been confirmed via repeated CT scans conducted under atmospheric conditions at a superficial gas velocity of 30 cm/s.
- At a high superficial gas velocity of 30 cm/s (at atmospheric pressure), sparger (gas distributor) effects on gas holdup and radial gas holdup profiles, which are the main factors in driving liquid recirculation, were insignificant in the 6.4-in. (16.2-cm) diameter column.
- The insignificant effect of the gas distributor on holdup is in agreement with the findings of Shollenberger *et al.* (1999), who experimented with a larger size column diameter of 18 in. (45 cm). Hence, the finding is column size independent.
- At these high superficial gas velocities, the entry region, where sparger effects might be present, was shorter than that of the two-column diameter.
- On the other hand, at a superficial gas velocity of 14 cm/s (at atmospheric pressure), sparger effects on gas holdup and radial gas holdup profiles were significant if spargers of vastly different design, such as perforated plate and single nozzle spargers, were compared.
- At the superficial gas velocity of 14 cm/s, the cross and nozzle spargers produced the same holdup profiles, which exhibited significantly different behavior compared to the perforated plate spargers:
  - Lower overall and cross-sectional average gas holdup
  - Insignificant axial variation of gas holdup at heights above the two-column diameter

- Industrially relevant spargers (e.g., cross and single nozzle spargers) produced the same holdup profiles, even at a superficial gas velocity of 14 cm/s and could be considered to have a small (negligible) sparger effect on holdup.

1. DISTRIBUTOR EFFECTS IN BUBBLE COLUMNS ON GAS HOLDUP VIA COMPUTED TOMOGRAPHY (CT)

Bubble column reactors are widely used in various areas, such as chemical processing, biotechnology and production of pharmaceuticals. One typical example is Fischer-Tropsch (FT) synthesis of liquid fuels from synthesis gas derived from coal. The commercial viability of such processes is dependent on high product throughput that can only be achieved at high superficial gas velocities. Overall gas holdup and its cross-sectional distribution are important parameters that govern the prevalent hydrodynamics in the column under particular operating conditions. The parameters that determine the gas holdup in a bubble column reactor are the operating conditions of the system and the reactor geometry, as well as the coalescing nature of the liquid phase.

In bubble column design and operation, another frequently asked question is whether sparger (gas distributor) design and configuration affect column performance. Knowing the answer to this question is important, since simpler sparger designs could represent significant cost savings in column construction. We have undertaken to address this question in a joint research effort with the Sandia National Laboratory. It is known that gas holdup radial profiles are the primary factor in driving liquid recirculation (due to radial buoyancy force differences), which in turn affects the extent of backmixing and reaction progress in the column. For this reason, at the Chemical Reaction Engineering Laboratory (CREL) at Washington University in Saint Louis, we have undertaken to obtain gamma ray CT scans of cross-sectional gas holdup profiles in the column. CT scans were acquired for a number of gas distributors at various axial locations and at different superficial gas velocities. In addition, overall gas holdup was obtained by comparison of the height of the two-phase mixture to the static liquid height.

Since operation of bubble columns at high superficial gas velocity is of the utmost interest, we addressed the issue of whether sparger design affects bubble column hydrodynamics in a major way under such operating conditions by conducting a set of experiments at a superficial gas velocity of 30 cm/s. To better understand the effect of sparger design on bubble column hydrodynamics, it was also necessary to investigate sparger effects at a lower gas superficial velocity of 14 cm/s. Traditional understanding of bubble column flow leads one to expect churn turbulent flow at a superficial gas velocity of 14 cm/s at atmospheric pressure in an air-water system. Hence, it is often assumed that at such conditions the sparger effects are minimal. In this study we show how large such effects can be.

1.1 Overall Plan

The study of the distributor effects on bubble column hydrodynamics has been undertaken in a collaborative effort with Sandia National Laboratory (SNL). Figure 1.1 shows the overall plan between the two laboratories, i.e., CREL and SNL.

1.2 Experimental Setup

Figure 1.2 shows the flowsheet for the system used in this study. The system is designed to handle a high flow rate of air up to 5000 SCFH at a pressure of up to 150 psig. All the equipment is designed to support operation at a maximum pressure of 200 psig. The bubble column is made of a stainless steel tube with an inner diameter of 0.162 m (6.4 in.) and a height of 2.5 m (8.2 ft).

As shown in Figure 1.2, a transparent glass window is situated at the top of the column and is named "blue eye." This window allows viewing of the system before the CT scan is started. The gas was dispersed into the column through different distributors. Figure 1.3 shows the various distributors used in this study. The first three distributors (D1-D3) were chosen in a collaborative effort with SNL to characterize the effect of sparger design on bubble column hydrodynamics. The following configurations of the spargers were employed:

A) Three distributors with 0.1% open area
- D1: Uniform perforated plate (163 holes of 0.4 mm ID, triangular pitch of 1 cm)
- D2: Cross sparger (4 holes of 2.6 mm ID)
- D3: Single nozzle (1 hole of 5.1 mm ID)

B) One distributor with 0.15% open area
- D4: Uniform perforated plate (163 holes of 0.5 mm ID, triangular pitch of 1 cm)

C) One distributor with 0.04% open area
- D5: Non-uniform perforated plate (61 holes of 0.4 mm ID located on 3 concentric circles 1.5 cm apart)

Compressed air was used as the gas phase after appropriate filtering, and for the liquid phase tap water (σ_L = 72 mN/m, μ_L = 993 μPa.s) was used. The experiments were conducted batchwise with respect to the liquid, but with a continuous flow of gas at ambient temperature (T = 20 °C). The static water height was in the range 120-150 cm. Table 1.1 lists the operating conditions employed in this work. The gas mixture was filtered before being introduced into the system. The gas flow rate was controlled by the rotameters. After exiting the bubble column, the gas passes through a backpressure regulator, which can be used to control the pressure in the column. It is then discharged into the atmosphere through the vent. Two pressure safety valves are mounted both at the top and bottom of the column to prevent accidental over-pressurization.

The gas holdup cross-sectional distribution was measured using the gamma ray scanner and associated tomography reconstruction algorithms developed in CREL and discussed by

Kumar (1994). The CREL scanner is a versatile instrument that enables the quantification of the time-averaged holdup distribution for two-phase flows under a wide range of operating conditions. The fan beam configuration of the scanner consists of an array of NaI detectors 5 cm in diameter (5 detectors were used in this study), and an encapsulated 100 mCi Cs^{137} source located opposite the center of the array of detectors. The measurements can be made at different axial locations, which allows quantification of the effects of operating conditions on the gas holdup distribution.

1.3 Measurements Performed

Overall gas holdup was determined by comparing the height of the two-phase mixture for the column in operation to the static liquid height. Presented below, radial gas holdup profiles at various axial locations were obtained by azimuthal averaging of the CT scans performed at those elevations. The gamma ray scanner developed in CREL and discussed by Kumar (1994) was used. The spatial resolution of the scanner was about 4 mm, and the density resolution was better than 0.05 g/cm^3.

1.4 Results and Discussion

A) Radial Holdup Profiles

First, we established the excellent reproducibility of the radial gas holdup profiles generated from the CT scans for a superficial gas velocity of 30 cm/s. Figure 1.4 exhibits the gas holdup radial profile obtained with distributor 4 at the elevation of z/D = 5.5 on three different days. The bounds for the 95% confidence interval, consisting of two standard deviations on each side of the mean, were well within ± 2% at every radial location, except at the points close to the wall, which were within ± 5%. It was not reasonable to expect that various distributors could produce gas holdup profiles within the range of reproducibility of a single distributor. We were not looking for identical behavior among distributors, but for insignificant differences in the hydrodynamics due to different distributors. For this reason, it was decided to plot the radial holdup profiles, $\varepsilon_{gi}(r)$, for all distributors taken at the same elevation. We then calculated the mean at each radial location $\varepsilon_g(r) = \sum_{i=1}^{N} \varepsilon_{gi}(r) \Big/ N$ and determined the distributor effect to be insignificant if $\varepsilon_{gi}(r)$ lay within the range from 0.95 $\varepsilon_g(r)$ to 1.05 $\varepsilon_g(r)$. This represented a narrow (less than ± 5%) band around the mean.

A.1 <u>Ug = 30 cm/s</u>

Figures 1.5, 1.6 and 1.7 display the radial gas holdup profiles at Ug = 30 cm/s for distributors D1, D2, D3, and D4 scanned at three different elevations of z/D = 2.1, 5.5 and 9.0, respectively. Also displayed in the figures is the lower bound of the allowable band at 0.95 $\varepsilon_g(r)$ and the upper bound at 1.05 $\varepsilon_g(r)$. All the data fall within this band except for some points for distributor D4, which had a different percent open area, and for two points near the

wall for distributor D1 at z/D = 9.0. Nevertheless, including data for D4, the maximum difference between the highest and the lowest holdup value observed at any radial location did not exceed 25%, and that maximum difference occurred in the wall region where holdup values were low, so that the actual absolute differences in holdup were not large. For the holdup data for dimensionless radius r/R <0.9, the maximum difference in recorded local holdup values did not exceed 10%. Based on this observation, and on examination of Figures 1.5 to 1.7, we concluded that for practical engineering purposes, the distributor effects were insignificant at a superficial gas velocity of 30 cm/s. This insignificant effect on gas holdup profile was maintained, even when the open area of the distributors was changed from 0.1% (D1, D2, D3) to 0.15% (D4). The only slight differences observed were slightly higher holdups at r/R greater than 0.9 for D4 with 0.15% open area compared to D1, D2, and D3 with 0.1% open area.

A.2 Ug = 14 cm/s

The same plots as those for Ug =30 cm/s are shown for all distributors at Ug = 14 cm/ in Figures 1.9, 1.10 and 1.11. As the figures illustrate, not all the distributors generated gas holdup profiles in the ± 5% band around the mean, and some differences were very significant, not only near the distributor zone, but also throughout the column. Noteworthy are the significant differences in gas holdup at a dimensionless radius location of r/R <0.8 in the core of the column.

In spite of the differences in the performance of the various distributors at Ug = 14 cm/s, distributors D2 and D3, which were the cross and the single nozzle spargers, respectively, generated almost identical gas holdup profiles for all elevations except at z/D = 9.0. The differences observed at z/D = 9.0 were most likely an artifact from the loss of liquid in the experiment with the cross sparger and drop of the gas-liquid interface near that elevation. This gave erratic holdup readings. The behavior of D2 and D3 was significantly different even from distributor D1, which had the same percent open area, but was a uniform perforated plate. Since perforated plates are rarely employed for industrial systems (spargers similar to D2 and D3 are preferred), for industrially important spargers, the effect of sparger design is negligible, even at a superficial gas velocity of 14 cm/s. Nevertheless, considering all the spargers evaluated in this study, sparger design does have a significant influence on gas holdup, even under operating conditions that are normally taken to be in the churn-turbulent regime.

In addition, when the radial gas holdup distribution trends for three perforated plate distributors (D1 - uniform, 0.1 POA; D4 - uniform, 0.15 POA; D5 - non-uniform, 0.04 POA) are compared, the holdup obtained using D4 is systematically higher than that from D1 at all radial locations. This is probably due to the same distribution of orifices on the perforated plates in the two cases, one with larger size orifices (0.5 mm for D4) and the other with smaller size orifices (0.4 mm for D1). The holdup obtained with D5 is lower than that obtained with D1 probably because of a lower percent open area (POA); however, there is no clear trend in the differences at various radial locations.

In conclusion, since radial holdup profiles drive liquid recirculation, the same holdup profiles should yield the same recirculation pattern, provided the turbulence structure, represented in the simplest fashion by a mixing length or turbulent kinematic viscosity, is the same. Computer Automated Radioactive Particle Tracking (CARPT) studies are being planned to determine whether the same radial holdup profiles resulted in the same liquid recirculation and turbulent kinetic energy patterns.

B) Axial Holdup Variation

The axial variation in the radial gas holdup profiles was examined. For the four distributors (D1-D4) investigated at Ug=30 cm/s, the axial variation is shown in Figures 1.12, 1.13, 1.14 and 1.15, respectively. These figures indicate that the radial gas holdup profile is not a function of axial position (except for points at r/R >0.85 for some distributors at z/D = 2.1). This implies that the entry region at this superficial gas velocity is confined to about two column diameters.

Figures 1.15 to 1.19 show gas holdup radial profiles at different elevations for all distributors at Ug = 14 cm/s. From Figures 1.15, 1.18 and 1.19, which relate to uniform and non-uniform perforated plate spargers, one can clearly see a significant axial variation. Also observable is a consistent trend for all three perforated plate distributors, in which gas holdup uniformly decreases with height. This implies that at this superficial gas velocity, the primary bubble size at the distributor is smaller than the secondary (stable) bubble size (Joshi *et al*., 1998). Barring the discrepancy observed at z/D = 9.0 for the cross sparger (D2) as mentioned earlier, Figures 1.16 and 1.17 indicate that there is relatively insignificant variation in axial gas holdup for spargers D2 and D3. This observation can be explained in terms of the stable bubble size, which is attained relatively close to the sparger, implying that the sparger zone for these two distributors is confined to less than two column diameters.

C) Overall Holdup

Overall holdup is obtained in two ways. Radial holdup profiles obtained by the CT scan are averaged in a cross section to obtain a cross-sectionally averaged holdup, $\bar{\varepsilon}_{gi}(z)$, at the desired elevation z for each distributor (i = 1, 2, 3, 4, 5).

$$\bar{\varepsilon}_{gi}(z) = \frac{2}{R^2}\int_0^R r\varepsilon_{gi}(r)\, dr \qquad (1)$$

These cross-sectional average values are interpolated between z/D = 2.1 to z/D = 9.0 using cubic splines and are axially averaged to obtain average total holdup.

$$\varepsilon_{gi,CT} = \frac{1}{(9.0-2.1)}\int_{z/D=2.1}^{z/D=9.0} \bar{\varepsilon}_{gi}(z/D)\, d(z/D) \qquad (2)$$

Cross-sectional averaged holdups at three elevations and axially averaged holdups determined from CT scans at Ug = 30 and 14 cm/s, as described above, are listed in Tables

1.2 and 1.3, respectively. Also shown in the tables is the overall column holdup ε_{gi} for each distributor (i = 1 to 5). Overall holdup was obtained by dividing the difference in dynamic height of the two-phase mixture and static liquid height by the static liquid height (Eq. 3).

$$\varepsilon_{gi} = \frac{H_{di} - H_s}{H_s} \qquad (3)$$

Due to the inherent inaccuracies in firmly establishing the dynamic liquid height for the column in operation, these holdup values can be subject to errors of ± 10 %. Table 1.2 reveals that the difference between CT-determined average holdup and average column holdup is always well within 10%. It is also clear from comparison of columns 5 and 6 in the table that column holdup is always higher than the CT estimate average. This is to be expected, as the holdup in the sparger region, which is not measured by CT, is higher than the holdup in the fully developed flow region. CT captures the holdup only in the fully developed zone, while the overall column holdup captures the contribution of all the zones.

However, at Ug = 14 cm/s, by the similar analysis of columns 5 and 6 in Table 1.3, one can see that the CT determined average is higher than the column average for the cross and single nozzle spargers (D2 and D3). This is to be expected since the bubble size at the distributor should be much larger for these spargers than the stable bubble size, resulting in a lower holdup near the distributor. Therefore, the column average holdup is expected to be lower compared to the CT-determined average, which is based on holdup values outside the distributor region. In addition, the column average holdup for all the perforated plate distributors is higher than the CT-determined average, indicating a higher gas holdup in the distributor zone, with the primary bubble size being much smaller than the stable bubble size.

D) Comparison of Sparger Effects for Ug = 14 cm/s with Ug = 30 cm/s

Figures 1.20 and 1.21 compare the variation in gas holdup profiles due to different spargers at the two superficial gas velocities investigated in this study. From these two figures, it can be clearly seen that sparger effects are minimal for Ug = 30 cm/s. This is indicated by the narrow band of ± two standard deviations, whereas this is not the case for Ug = 14 cm/s. Figure 1.20 also indicates that the normalized deviations are the largest near the wall.

E) Cross-Sectional Gas Holdup Distribution

Figures 1.22 and 1.23 show the representative cross-sectional gas holdup distribution for the cross sparger (D2) at Ug = 14 and 30 cm/s, respectively, scanned at z/D = 5.5. A gradual variation in the color shades for the gas holdup from the column center to the wall indicates a change in gas holdup values. As can be seen from these two figures, the time-averaged gas holdup distribution is nearly axisymmetric and indicates more gas in the column center with gradual decay towards the wall.

F) Comparison with Earlier Work

It is interesting to compare the results obtained in this study with the work performed earlier by Kumar (1994) and Degaleesan (1997). Using the CT scanner at CREL, Kumar (1994) studied the effect of distributor types on gas holdup distribution in an air-water system using a column with a slightly larger diameter of 19 cm. In his study, Kumar used the following spargers:

- Perforated plate (166 holes of 0.33 mm ID, square pitch, 0.05% open area)
- Bubble cap distributor
- Cone distributor

However, only two relatively low superficial gas velocities (5 and 8 cm/s) were investigated. The conclusions from that study were that the gas holdup obtained with a perforated plate distributor is higher than that obtained from the bubble cap and cone distributors. This observation is similar to those at Ug=14 cm/s in the current study, even though the employed superficial gas velocity is significantly higher.

Degaleesan (1997) investigated the effect of gas distributors on liquid recirculation using the same experimental setup as that of Kumar (1994). The Computer Automated Radioactive Particle Tracking (CARPT) technique was employed to assess the level of liquid recirculation and turbulence at a superficial gas velocity of 12 cm/s. It was found that the time-averaged axial liquid velocity, for both bubble cap and cone distributors, was lower compared to that for the perforated plate. This was explained in terms of relatively larger bubbles that are formed when a bubble cap or a cone distributor is used, as opposed to a perforated plate distributor. The presence of large bubbles was reported to result in lower overall gas holdup and higher turbulent kinetic energy, which in turn generates larger scale turbulence. More details on that study can be found in the 14^{th} and 15^{th} Quarterly Reports. This indirectly implies that the gas holdup using the perforated plate distributor was significantly higher than that from bubble cap and cone distributors, even at a superficial gas velocity of 12 cm/s. This observation is in agreement with the measurements reported in this study at a comparable Ug of 14 cm/s.

Conclusions

The study at a high superficial gas velocity of 30 cm/s under atmospheric condition confirms the findings of Shollenberger *et al.* (1999) that in churn-turbulent flow, the gas distributor does not affect gas holdup or the radial gas holdup profile. Moreover, the entry length is confined to $z/D \leq 2$. However, at a superficial gas velocity of 14 cm/s, at which the regime of bubble column operation is usually reported to be churn-turbulent, significant radial gradients in the gas holdup profile are observed with a greater concentration of gas in the column center. Therefore, it was anticipated that sparger design would have a minimal effect under such operating conditions. On the contrary, the findings from this study indicate that there is a significant variation in gas holdup from perforated-plate type distributors to nozzle type distributors. Such differences were not observed at a superficial gas velocity of 30 cm/s, at which the turbulent intensities are much higher. Whether the sameness of the radial gas

holdup profile at Ug = 30 cm/s implies the same or similar liquid recirculation and mixing patterns is the subject of future research

At a superficial gas velocity of 14 cm/s, the perforated plate spargers exhibit a similar behavior of axially decreasing gas holdup, whereas the cross and single-nozzle spargers show an insignificant variation in gas holdup at heights above two-column diameter. In addition, it is interesting to note that Kumar (1994) and Degaleesan (1997) also observed similar trends when using perforated-plate distributors compared to nozzle type distributors in a different column geometry.

Since the transition to the churn-turbulent regime is delayed at elevated pressures, future studies should investigate whether a superficial gas velocity of 14 cm/s still represents the churn-turbulent regime (indicated by steeper radial gas holdup profiles) and what effect spargers have at such conditions. We believe that our findings at a superficial gas velocity of 30 cm/s will be confirmed as well at elevated pressures in future studies, as long as the churn-turbulent regime is maintained.

References

Degaleesan, S., "Turbulence and liquid mixing in bubble columns," *Ph.D. Thesis*, Washington University, St. Louis (1997).

Joshi, J. B., U. Parasu Veera, Ch. V. Prasad, D. V. Phanikumar, N. S. Deshphande, S. S. Thakre, and B. N. Thorat, "Gas holdup structure in bubble column reactors," *PINSA*, **64**, A, 4, 441-567 (1998).

Kumar, S. B., "Computed tomographic measurements of void fraction and modeling of the flow in bubble columns," *Ph.D. Thesis*, Florida Atlantic University (1994).

Shollenberger, K. A., J. R., Torczynski, and D. L. George, "Monthly progress report for collaborative sparger study," submitted to Air-Products (June 2, 1999).

Table 1.1 Experimental Conditions Used

Column ID, cm (in.)	16.2 (6.4)
Ug (Air), cm/s	14, 30
Liquid (Water)	Batch
Pressure, MPa (atm)	0.1 (1)
Temperature, °C	25
CT scan levels from the distributor, cm	34, 89, 145
z/D	2.1, 5.5, 9.0

Table 1.2 Cross-Sectional Averaged Gas Holdup and Overall Gas Holdup at Ug = 30 cm/s and Atmospheric Pressure

	Cross-sectional averaged gas holdup					% difference between
Sparger	z/D = 2.1	z/D = 5.5	z/D = 9.0	$\varepsilon_{g,CT}$	ε_g	$\varepsilon_{g,CT}$ & ε_g
1	0.277	0.263	0.285	0.269	0.293	9.0
2	0.268	0.263	0.272	0.265	0.281	5.9
3	0.289	0.259	0.270	0.266	0.284	7.0
4	0.300	0.2817	0.2924	0.287	0.300	4.7
Avg. ± 2SD	0.283 ± 0.028	0.267 ± 0.021	0.280 ± 0.022	0.272 ± 0.020	0.290 ± 0.017	6.7 ± 3.6

Table 1.3 Cross-Sectional Averaged Gas Holdup and Overall Gas Holdup at Ug = 14 cm/s and Atmospheric Pressure

	Cross-sectional averaged gas holdup					% difference between
Sparger	z/D = 2.1	z/D = 5.5	z/D = 9.0	$\varepsilon_{g,CT}$	ε_g	$\varepsilon_{g,CT}$ & ε_g
1	0.249	0.211	0.196	0.215	0.225	4.7
2	0.183	0.180	0.184	0.181	0.179	1.1
3	0.170	0.187	0.189	0.188	0.180	4.1
4	0.288	0.264	0.229	0.262	0.277	5.7
5	0.236	0.205	0.193	0.208	0.224	7.8
Avg. ± 2SD	0.229 ± 0.086	0.209 ± 0.067	0.198 ± 0.036	0.211 ± 0.074	0.207 ± 0.049	4.7 ± 4.9

Overall Plan For CREL and Sandia

CREL, Washington University

- Perform quick check of the sparger effects at Ug = 30 cm/s, and P = 1 atm via
  - **CT and overall gas holdup**
  - **CARPT**
  - **4-points optical probe**
- Column ID = 6.4” (16.2 cm)
- Air-water system
- Spargers specifications

  0.1 Percent Open Area (POA)

  Configuration
  - **Cross Sparger (4 holes, 2.6 mm)**
  - **Uniform Perforated Plate (163 holes, 0.4 mm)**
  - **Single Nozzle (1 hole, 5.1 mm)**

Sandia National Laboratory

- Perform quick check of the sparger effects at Ug = 30 cm/s, and P = 1 atm via
  - **Overall gas holdup**
  - **γ-ray densitometry-tomography (GDT)**
- Column ID = 19” (48.3 cm)
- Air-Drakeol system
- Spargers specifications

  0.1 *Percent Open Area (POA)*

  Configuration
  - **Cross Sparger (96 holes, 1.6 mm)**
  - **Cross Sparger (24 holes, 3.2 mm)**
  - **Cross Sparger (4 holes, 7.5 mm)**

Figure 1.1 Overall Plan for Chemical Reaction Engineering Laboratory (CREL) and Sandia National Laboratory

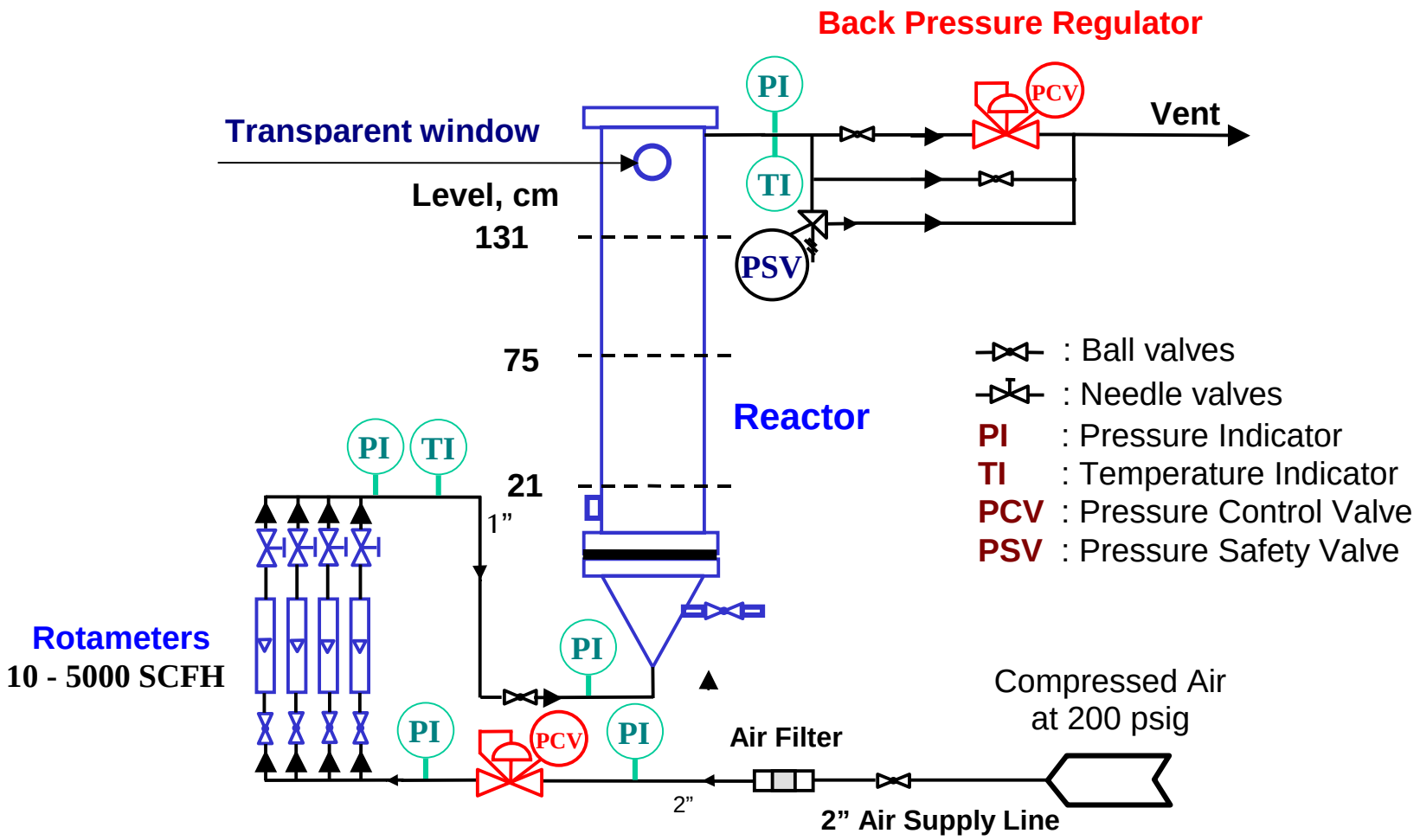

Figure 1.2 Schematic Diagram of the Experimental Setup

D1

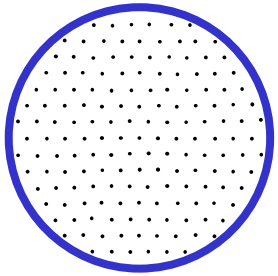

Porosity *= 0.1 %*
163 holes of 0.4 mm ID
Equilateral triangle 1 cm apart

D2

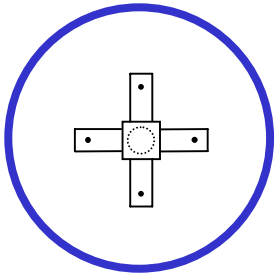

Porosity *= 0.1 %*
4 holes of 2.6 mm ID
Distributed on a cross

D3

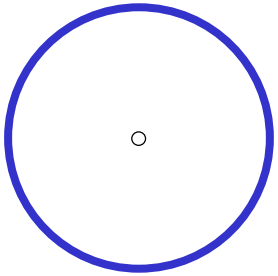

Porosity *= 0.1 %*
Single hole of 5.1 mm ID
Located in the center

D4

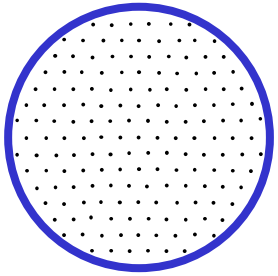

Porosity *= 0.15 %*
163 holes of 0.5 mm ID
Equilateral triangle 1 cm apart

D5

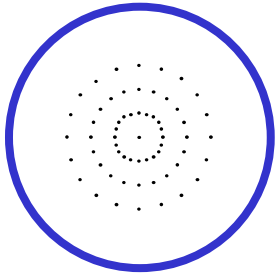

Porosity *= 0.04 %*
61 holes of 0.4 mm ID
Circular rings 1.5 cm apart

Figure 1.3 Sparger Design and Configurations

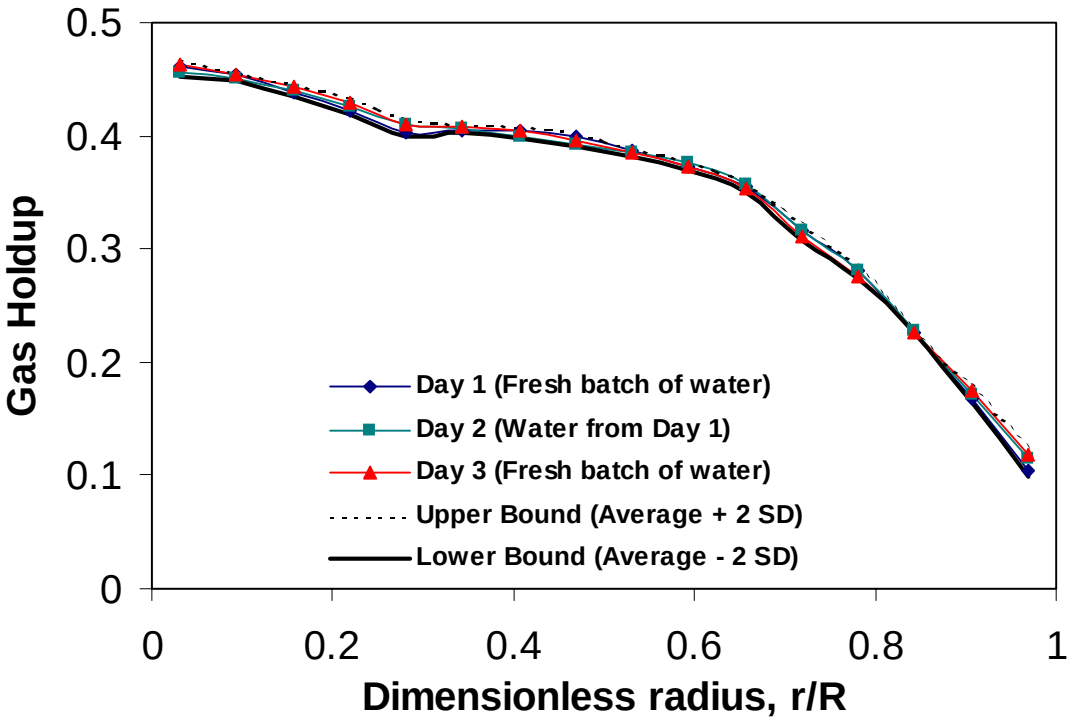

Figure 1.4 Reproducibility Plots using D4, Different Batches of Water on Three Different Days

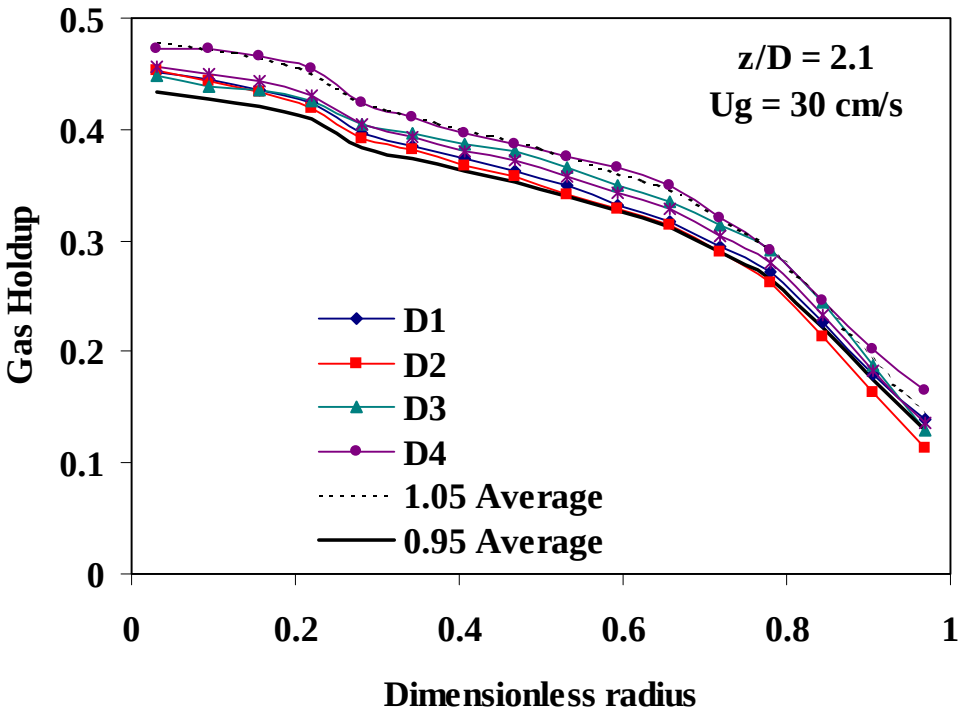

Figure 1.5 Effect of Spargers at Ug = 30 cm/s at Scan Level z/D = 2.1

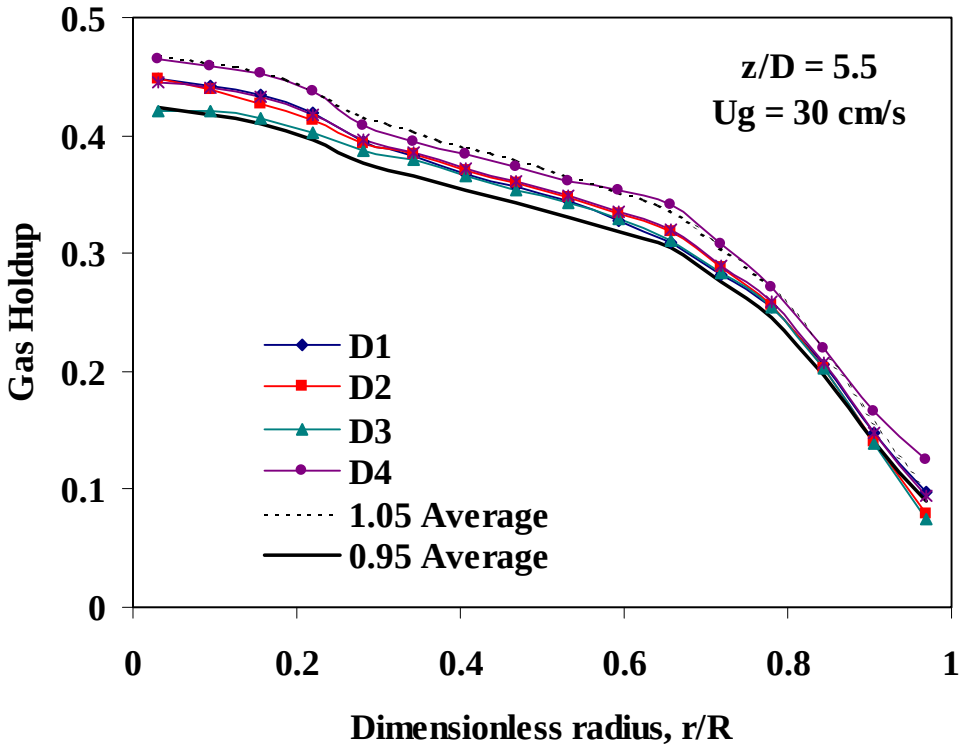

Figure 1.6 Effect of Spargers at Ug = 30 cm/s at Scan Level z/D = 5.5

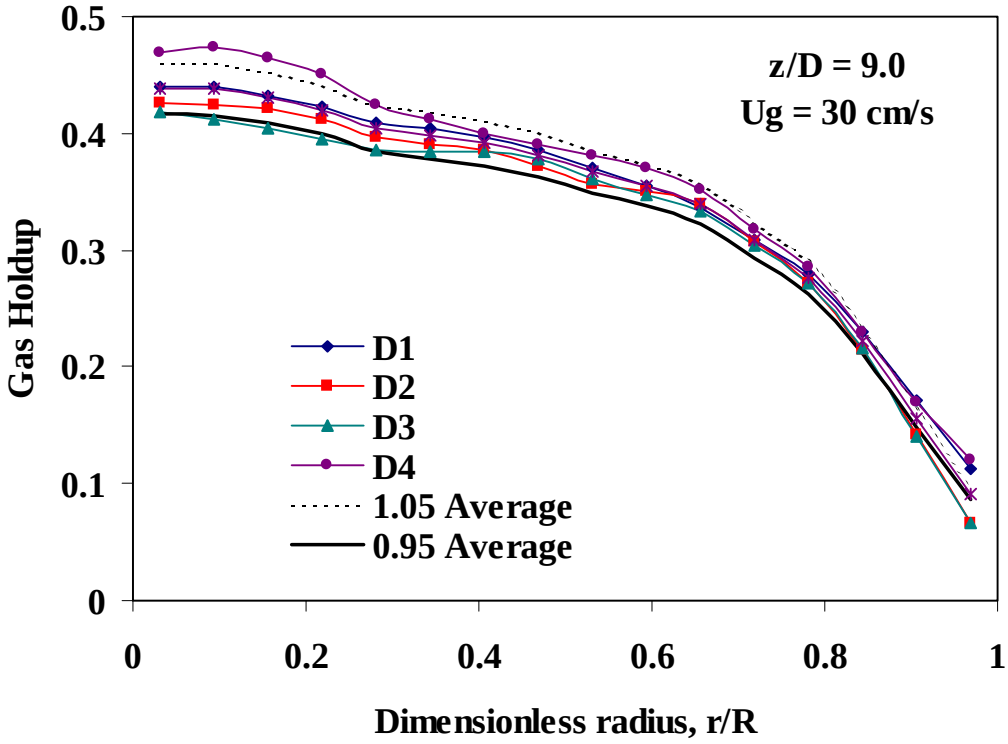

Figure 1.7 Effect of Spargers at Ug = 30 cm/s at Scan Level z/D = 9.0

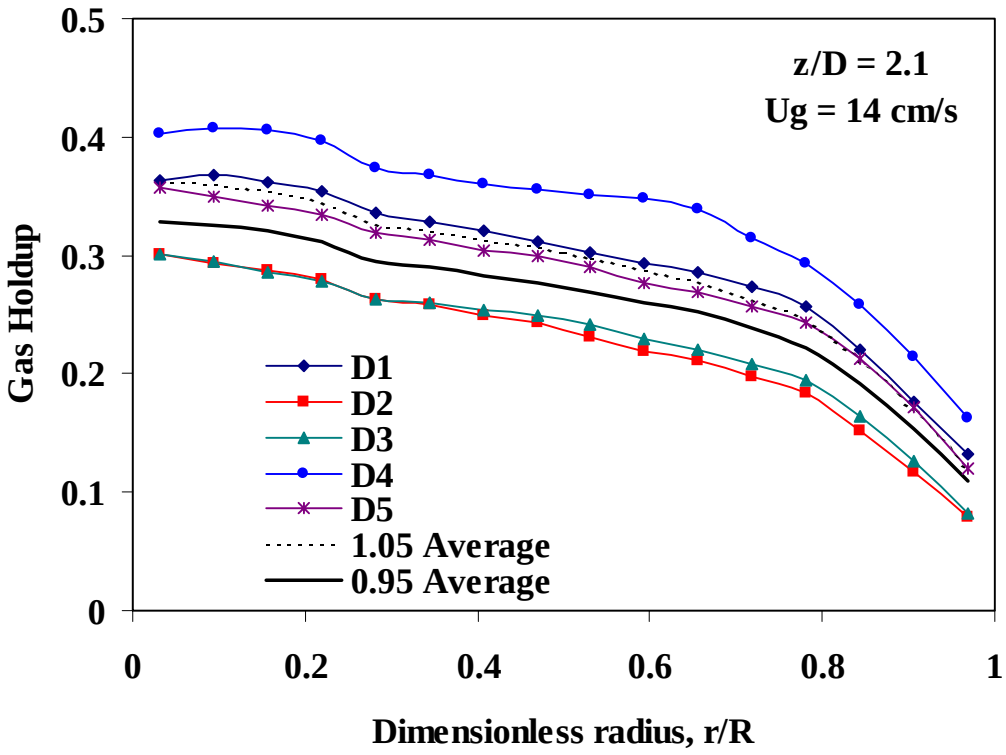

Figure 1.8 Effect of Spargers at Ug = 14 cm/s at Scan Level z/D = 2.1

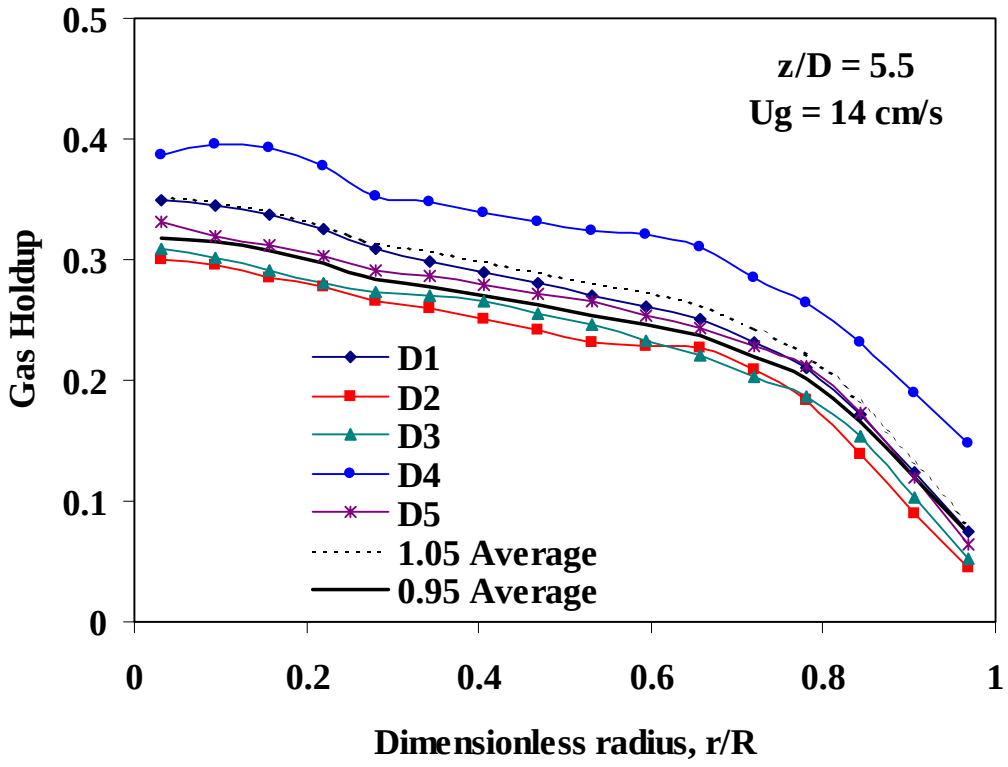

Figure 1.9. Effect of Spargers at Ug = 14 cm/s at Scan Level z/D = 5.5

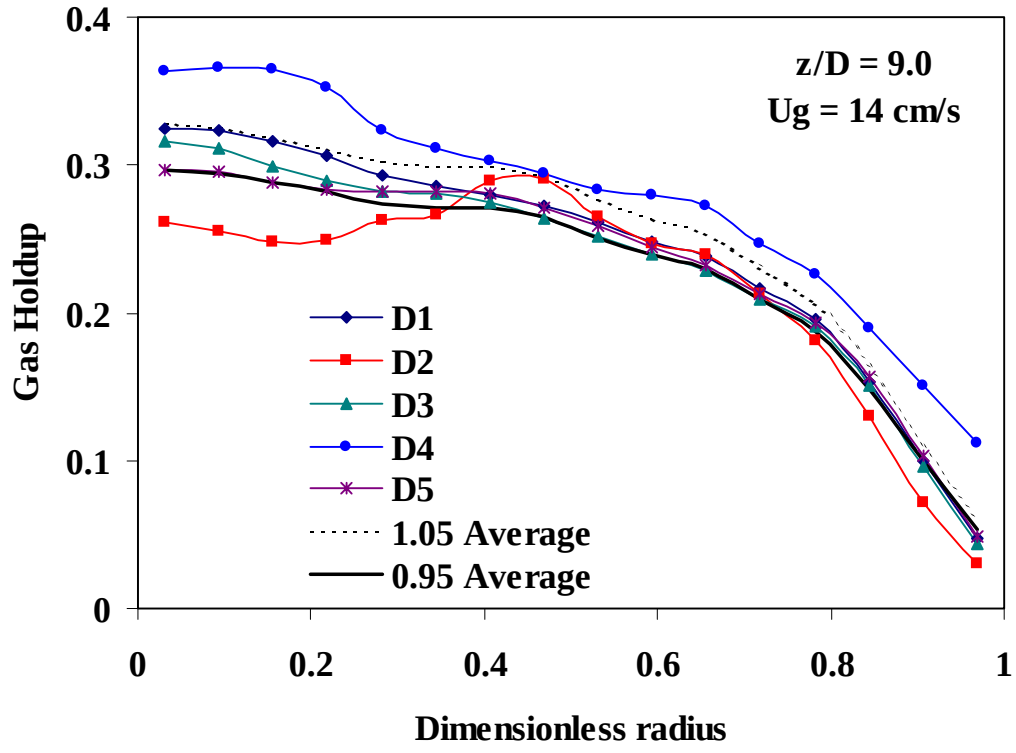

Figure 1.10 Effect of Spargers at Ug = 14 cm/s at Scan Level z/D = 9.0

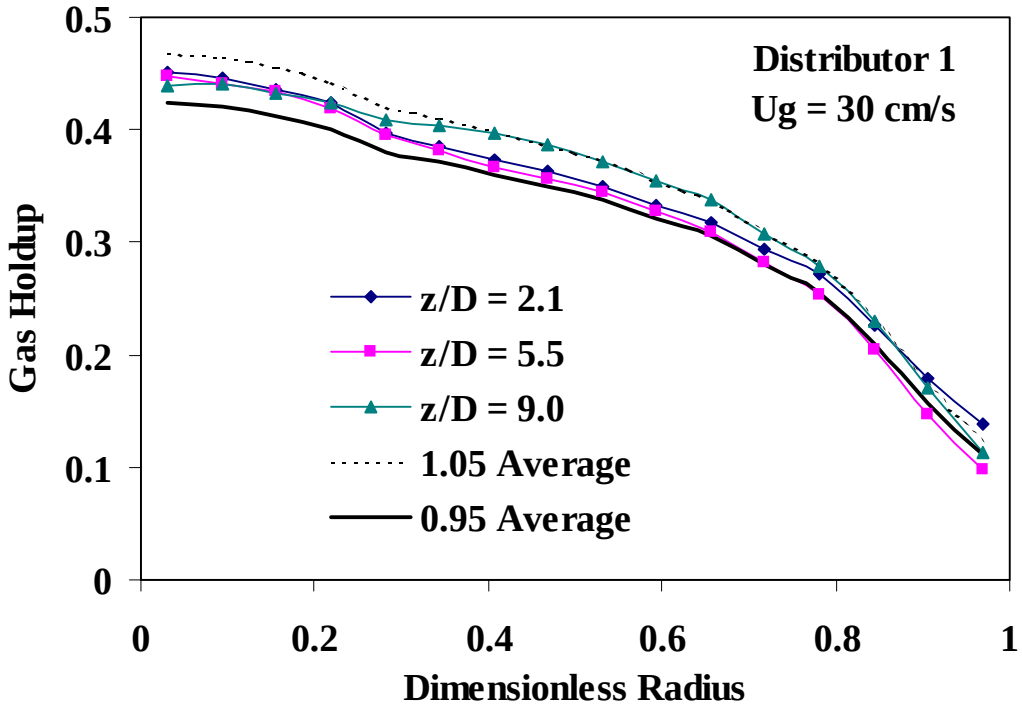

Figure 1.11 Axial Variation of Gas Holdup for Distributor 1 at Ug = 30 cm/s

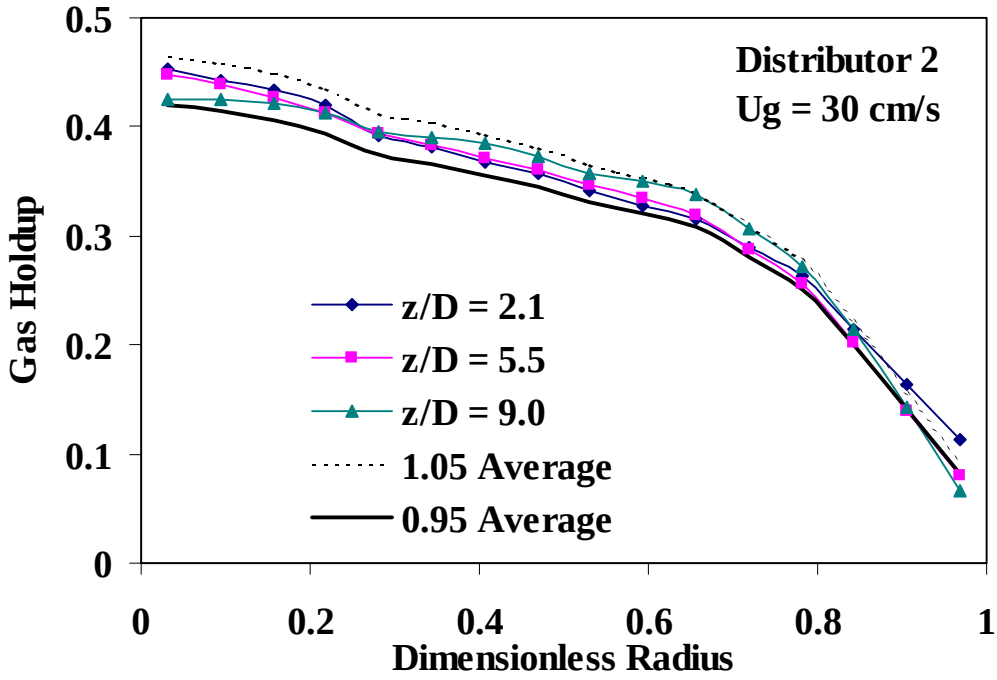

Figure 1.12 Axial Variation of Gas Holdup for Distributor 2 at Ug = 30 cm/s

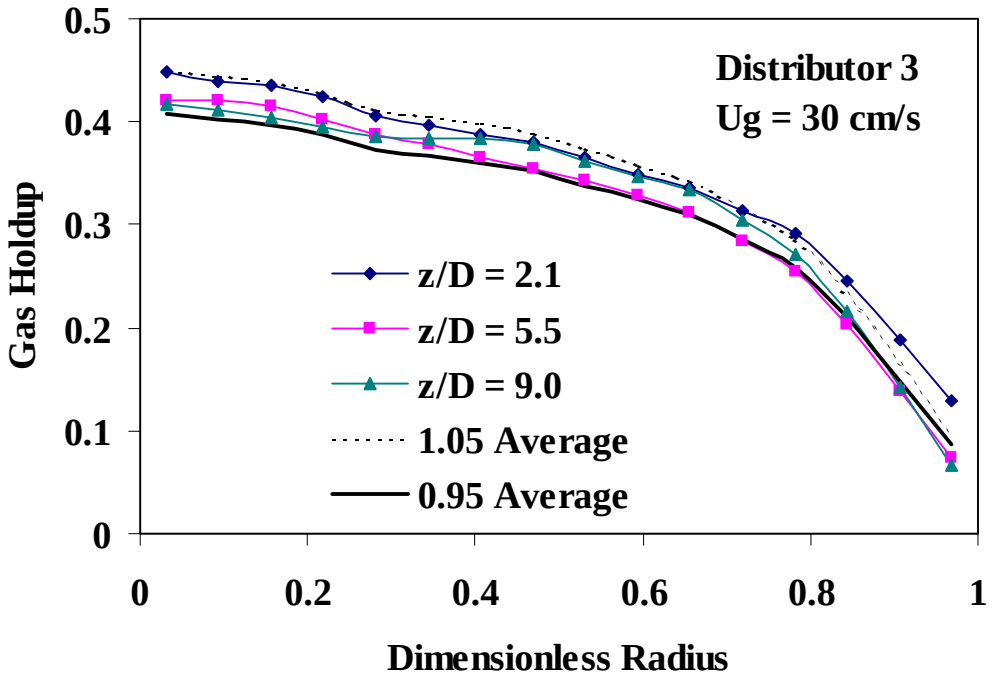

Figure 1.13 Axial Variation of Gas Holdup for Distributor 3 at Ug = 30 cm/s

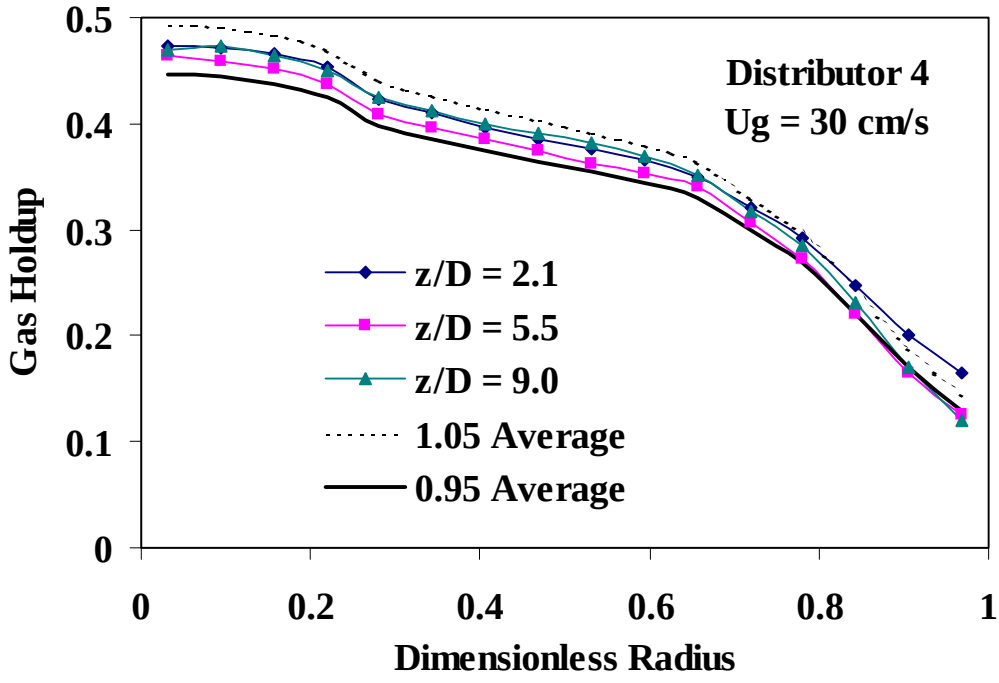

Figure 1.14 Axial Variation of Gas Holdup for Distributor 4 at Ug = 30 cm/s

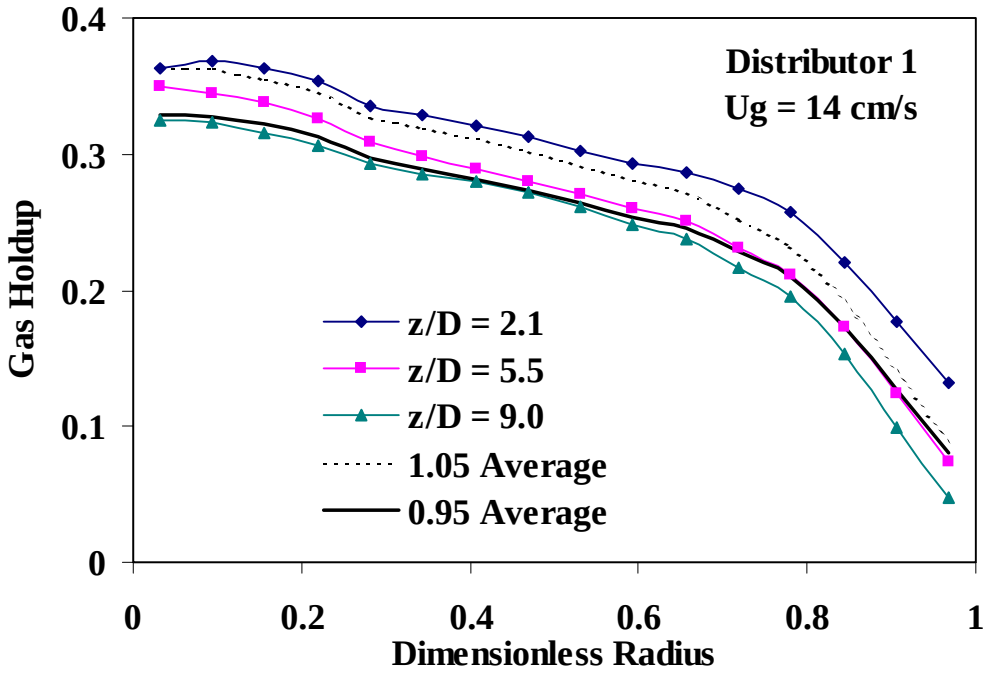

Figure 1.15 Axial Variation of Gas Holdup for Distributor 1 at Ug = 14 cm/s

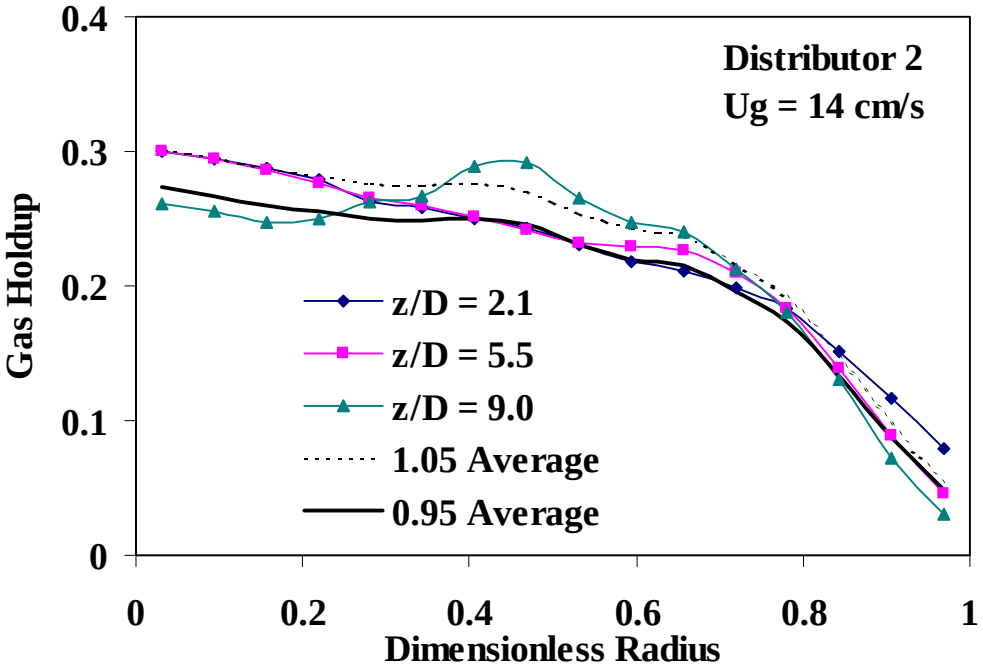

Figure 1.16 Axial Variation of Gas Holdup for Distributor 2 at Ug = 14 cm/s

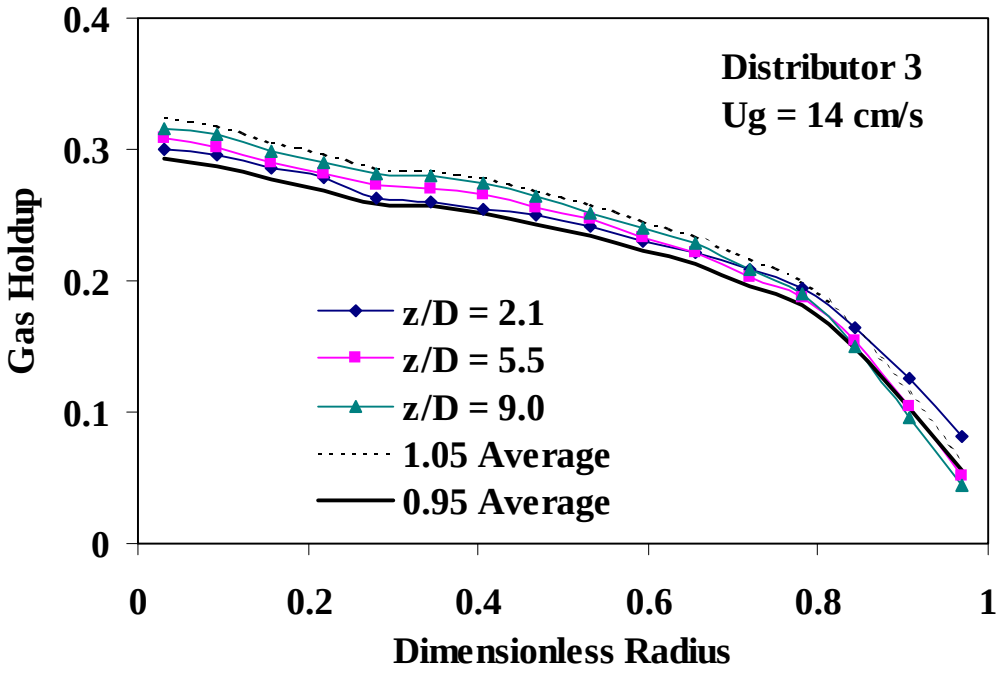

Figure 1.17 Axial Variation of Gas Holdup for Distributor 3 at Ug = 14 cm/s

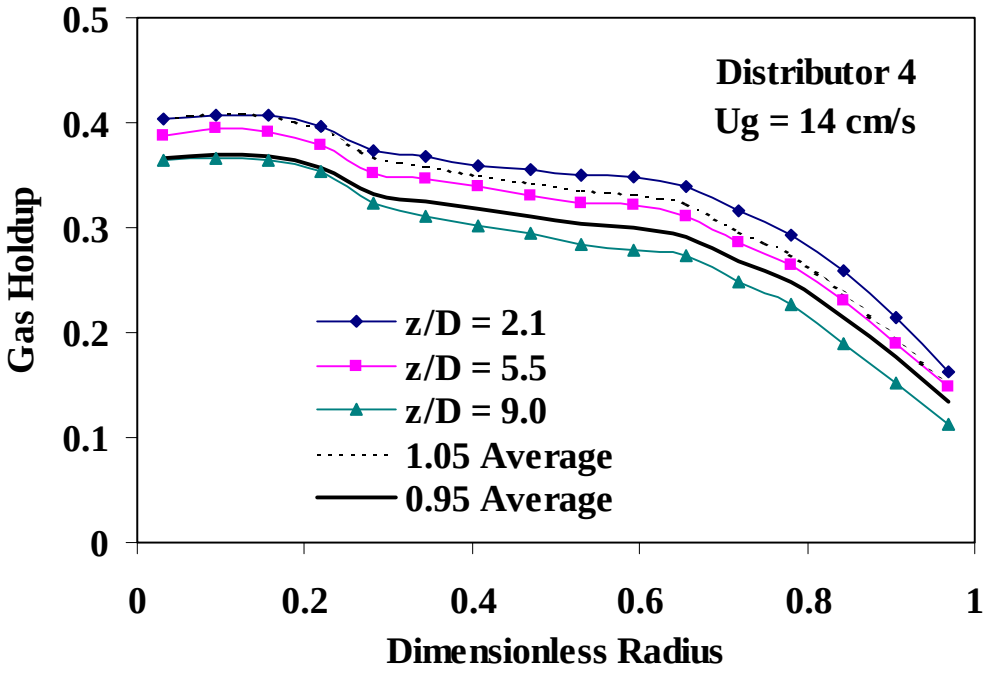

Figure 1.18 Axial Variation of Gas Holdup for Distributor 4 at Ug = 14 cm/s

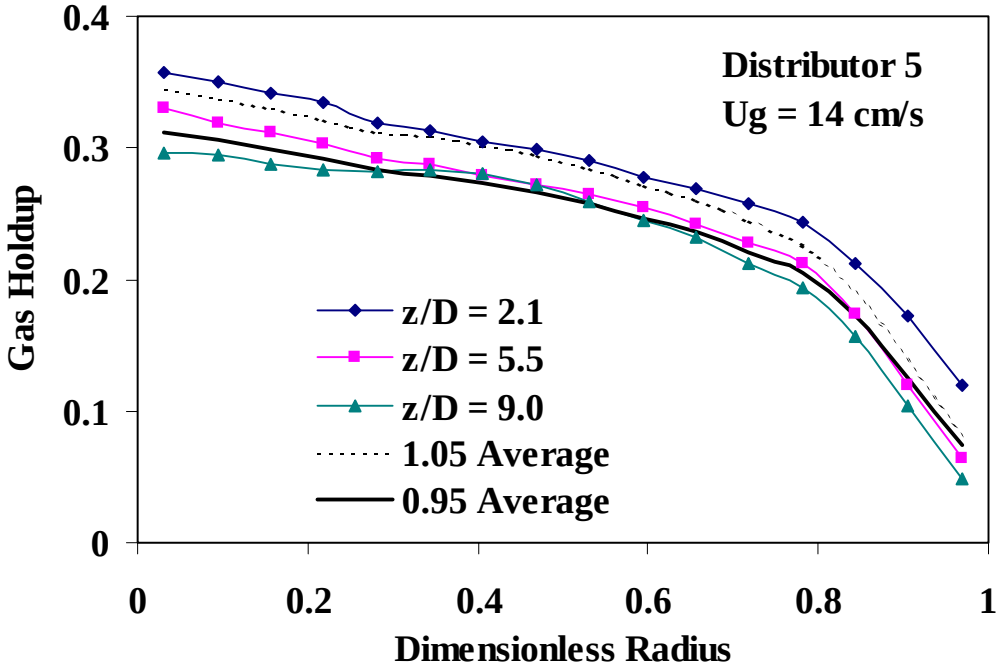

Figure 1.19 Axial Variation of Gas Holdup for Distributor 5 at Ug = 14 cm/s

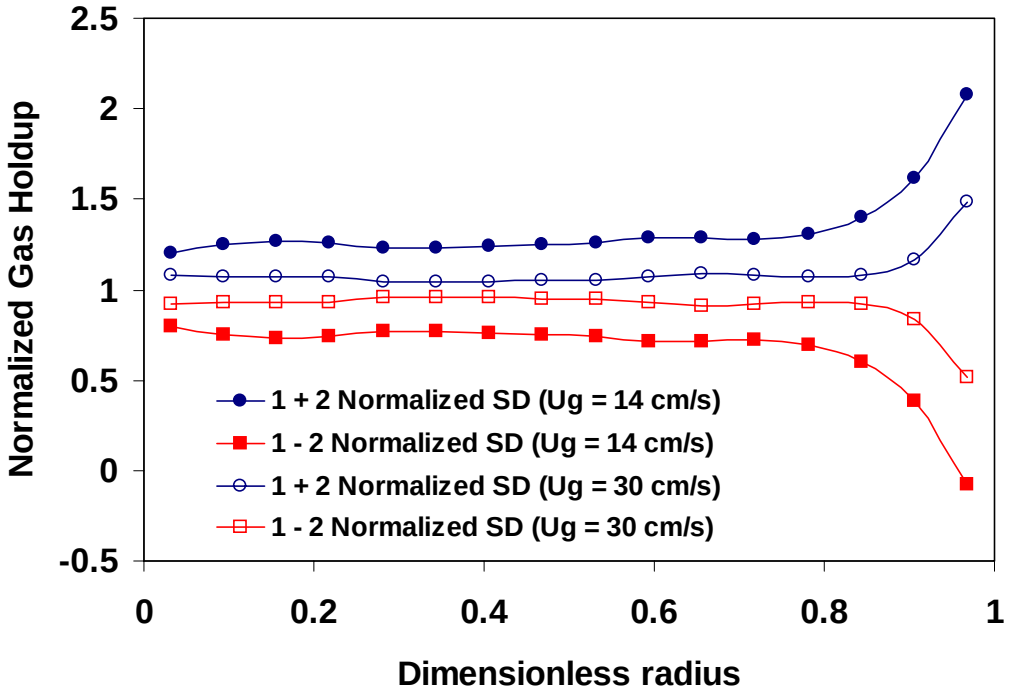

Figure 1.20 Comparison of Normalized Gas Holdup Variation due to Different Spargers at Ug = 14 cm/s and 30 cm/s

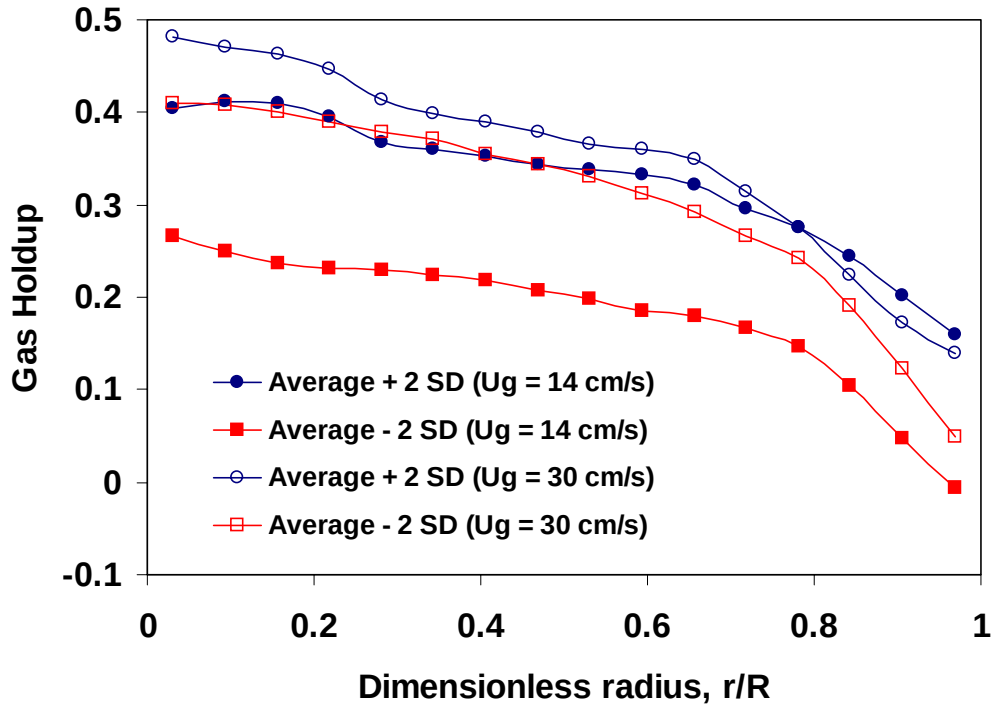

Figure 1.21 Comparison of Gas Holdup Variation due to Different Spargers at Ug = 14 cm/s and 30 cm/s

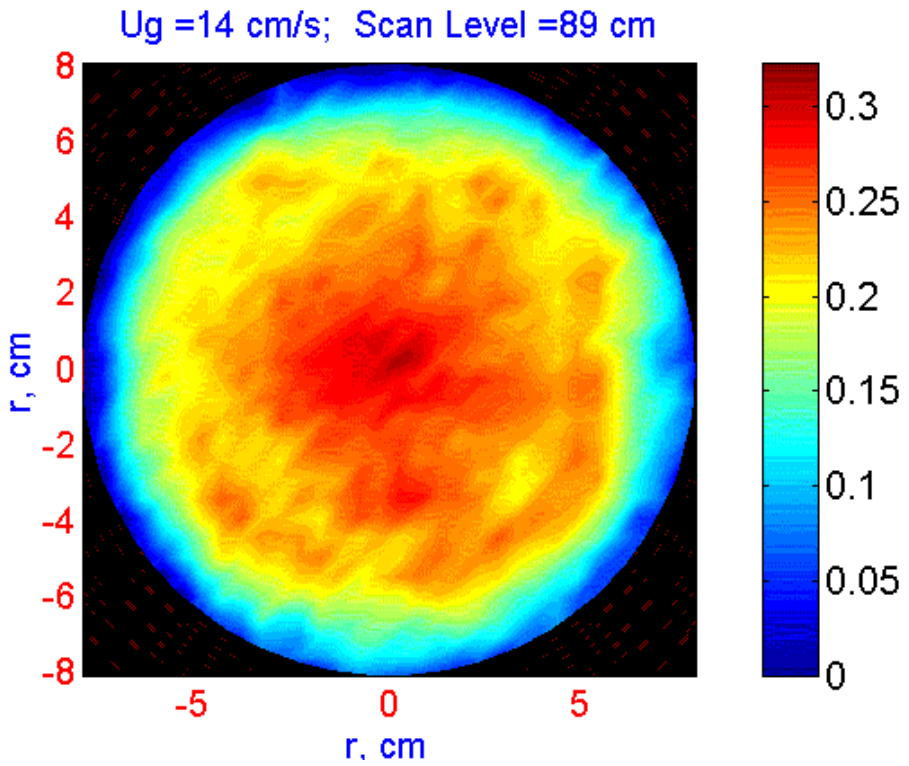

Figure 1.22 Cross-Sectional Time-Average Gas Holdup Distribution for the Cross Sparger (D2) at Ug = 14 cm/s at z/D = 5.5

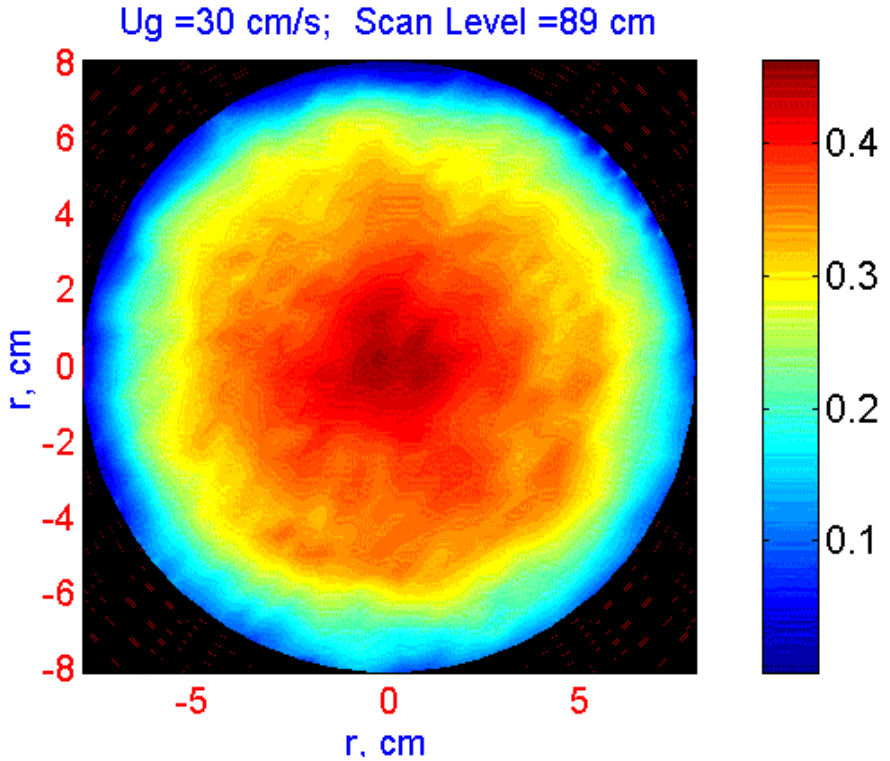

Figure 1.23 Cross-Sectional Time-Average Gas Holdup Distribution for the Cross Sparger (D2) at Ug = 30 cm/s at z/D = 5.5